Floral Stage Optimization and Immune Evasion Enhance *Agrobacterium*-Mediated Genome Editing in *Arabidopsis*

Running title: Optimization for *Arabidopsis* Floral Dip Transformation

Mao-Sen Liu†, Teng-Kuei Huang†, Yi-Chieh Wang, Si-Chong Wang, Chih-Hang Wu, Chih-Horng Kuo, Erh-Min Lai*

Institute of Plant and Microbial Biology, Academia Sinica, Taipei, Taiwan

*Correspondence (Tel: +886-2-2787-1158; email: emlai@gate.sinica.edu.tw)

†These authors contributed equally to this work

Author details, including affiliation and email address

msliu@gate.sinica.edu.tw; tengkueih@gmail.com; ejw@gate.sinica.edu.tw; sky972sakura@gmail.com; wuchh@gate.sinica.edu.tw; chk@gate.sinica.edu.tw; emlai@gate.sinica.edu.tw

ORCID ID

ORCID ID of the authors: M.-S.L. 0000-0003-0324-5866; T.-K.H. 0000-0001-7369-3678; S.-C.W. 0000-0002-6192-8844; C.-H.W. 0000-0003-1616-1872; C.-H.K. 0000-0002-2857-0529; E.-M.L. 0000-0003-3630-8683

Word counts: 5607 words (Introduction, Materials and Methods, Results, Discussion)

Number of figures: 7 (all to be published in colour)

Supporting information

SUMMARY

- *Agrobacterium*-mediated transformation via floral inoculation (AMT-FI) enables genetic engineering without tissue culture. It is widely used in the model plant *Arabidopsis thaliana*, yet its efficiency and broader applicability remain limited.
- Here, we used a dual-reporter system (RUBY and hygromycin resistance) to identify key floral stages and engineered *Agrobacterium* strains to evade plant immunity, leading to enhanced transient expression and genome editing.
- We determined that flowers opened at 6 day-post-inoculation (DPI) are optimal for high transformation efficiency, with nearly 100% of siliques harboring transformants. However, *Agrobacterium* infection induced ovule abortion, particularly in wild-type (Col-0) plants, whereas *efr* mutants lacking the EF-Tu receptor (EFR)-mediated pattern-triggered immunity (PTI) showed reduced ovule abortion. Notably, *efr* mutants exhibited more RUBY-positive ovules and significantly enhanced genome editing efficiency. Two engineered stealth *Agrobacterium* strains (AS201 and AS202) expressing a chimeric EF-Tu for evading recognition by EFR enhanced both transient transformation and genome editing efficiency. Remarkably, genome-edited T1 plants could be recovered based on phenotype or direct sequencing without the need for antibiotic selection when targeting flowers opened at 6 DPI.
- By integrating floral stage selection, immune evasion, and *Agrobacterium* engineering, this study provides a practical and versatile platform to advance plant genome engineering.

KEY WORDS

Arabidopsis, *Agrobacterium*, floral dip, plant immunity, genome editing, *Agrobacterium*-mediated transformation, EF-Tu, EFR

INTRODUCTION

Agrobacterium species are unique bacteria capable of cross-kingdom gene transfer, leading to diseases like crown gall or hairy root in a wide range of plant species (Hwang *et al.*, 2017; Lacroix & Citovsky, 2019). This remarkable ability has been harnessed in plant genetic engineering by replacing the oncogenes within T-DNA region of tumor-inducing plasmids with genes of interest (Suzuki *et al.*, 2009; Hooykaas, 2023). *Agrobacterium*-mediated transformation (AMT) has become a cornerstone technique in plant biology and the development of genetically modified organisms (GMOs) that stably express agricultural traits for crop improvements (Bevan, 1984; Gelvin, 2003).

Beyond enabling stable gene integration, AMT also supports transient expression of genome-editing machinery, allowing precise genome modifications. Since the T-DNA containing these editing components can be eliminated via chromosome segregation in subsequent generations, this strategy mitigates food safety concerns associated with GMOs (Pixley *et al.*, 2022).

Agrobacterium naturally infects somatic plant cells by responding to wound signals in roots or stems. Interestingly, it can also target germline tissues such as female gametophytes, which laid the foundation for the floral dip method widely used in *Arabidopsis thaliana* (Clough & Bent, 1998; Angulo *et al.*, 2023). This method, referred to here as *Agrobacterium*-mediated transformation by floral inoculation (AMT-FI), bypasses labor-intensive tissue culture, offering a more efficient transformation pathway. However, its application in species beyond *A. thaliana* has limited success (Bélanger *et al.*, 2024).

Although many plant factors that promote or suppress tumorigenesis and AMT have been identified, the genes involved in AMT-FI may be distinct (Hwang *et al.*, 2017; Lacroix & Citovsky, 2019; Weisberg *et al.*, 2023). Several *Arabidopsis* mutants or ecotypes resistant to root transformation remain susceptible to AMT-FI (Nam *et al.*, 1997; Mysore *et al.*, 2000). Notably, *polQ* mutants lacking DNA polymerase theta are deficient in T-DNA integration via AMT-FI, although their capability for stable transformation in roots remains debated (van Kregten *et al.*, 2016; Nishizawa-Yokoi *et al.*, 2021). These findings highlight that developmental processes may impose different requirements for successful transformation in germline and somatic cells.

Understanding the genetic and molecular basis of AMT-FI is crucial to expanding its utility across plant species.

Plant immunity plays a pivotal role in suppressing tumorigenesis and AMT efficiencies (Tiwari *et al.*, 2022; Dodds *et al.*, 2024). Upon *Agrobacterium* infection, plants recognize pathogen-associated molecular patterns (PAMPs) such as EF-Tu, flagellin, and cold-shock proteins by pattern-recognition receptors (PRRs), activating pattern-triggered immunity (PTI) that suppress transformation (Zipfel *et al.*, 2006; Wu *et al.*, 2014; Saur *et al.*, 2016; Wang *et al.*, 2018; Fürst *et al.*, 2020). Salicylic acid (SA) is a key defense hormone that reduces tumor formation and transient transformation (Anand *et al.*, 2008). Additionally, antimicrobial secondary metabolites, including glucosinolates and camalexin, restrict *Agrobacterium* infection at early and late stages, respectively (Shih *et al.*, 2018). These defense strategies collectively highlight the resilience of plants to counteract *Agrobacterium* infection and limit its transformation success.

In *Arabidopsis*, the EF-Tu receptor (EFR) plays a key role in recognizing *Agrobacterium* EF-Tu and inhibiting transient transformation (Zipfel *et al.*, 2006; Wu *et al.*, 2014; Wang *et al.*, 2018). However, EFR does not exhibit a significant impact on stable transformation or gene targeting efficiency (van Tol *et al.*, 2022; Yang *et al.*, 2023). To date, its influence on AMT-FI-mediated genome editing has not been fully elucidated.

In this study, we investigated the temporal and spatial localization of *Agrobacterium* cells and transformation events during AMT-FI in *A. thaliana.* A dual reporter system, combining a visible RUBY marker with a hygromycin resistance marker, was utilized to identify the floral tissues and stages most susceptible to AMT. Furthermore, we examined the impact of EFR-mediated PTI in transformation and genome-editing efficiencies. Our results revealed that AMT events peak in flowers opened at 6 day-post-inoculation (DPI), with *efr* mutants exhibiting significantly higher genome editing efficiency than Col-0. Moreover, we engineered two independent *Agrobacterium* strains expressing a chimeric EF-Tu, which further enhanced both transient expression and genome editing efficiency without significantly altering stable transformation frequency. These findings offer new strategies to facilitate AMT-FI-based genome editing in plants.

121

122 **MATERIALS AND METHODS**

123 **Plant materials and growth condition**

124 *Arabidopsis thaliana* Col-0, EF-Tu receptor (EFR) mutants, *efr*-1 (SALK_044334)
125 and *efr*-2 (SALK_068675) were used in this study. Seeds were sown in soil
126 (peatmoss:vermiculite:perlite = 12:1:1), germinated, and grown in a growth room
127 under conditions of 22 °C with 16h light/8h dark photoperiod.

128 **Bacterial growth condition**

129 For tracking *Agrobacterium* localization and transformation events, *Agrobacterium*
130 cells were cultured in 523 with appropriate antibiotics (Kado & Heskett, 1970). For
131 genome editing experiments, LB medium supplemented with appropriate antibiotics
132 was used. Freshly streaked out *Agrobacterium* colonies grown on 523 or LB agar
133 were cultured in the same medium (5 mL) for 2 days at 28 °C. The cultures were
134 subsequently diluted 1:1000 in 50 mL 523 or LB, grown for 22-24 hours, harvested
135 by centrifugation at 6000x g for 20 minutes. The cell pellets were resuspended in
136 infiltration medium (1/2 MS, 5% sucrose, 0.04% silwet-L77, 44 nM BAP and 200 μM
137 acetosyringone, pH=5.7) to OD_{600}=1.

138 **Plasmid construction**

139 Plasmid and primer information are listed in Table S1 and S2, respective.
140 35S::RUBY plasmid (Addgene#160908) which provided a visible RUBY reporter and
141 hygromycin resistance (Hyg^R) reporter was obtained from Addgene.

142 The gentamycin resistance gene (Gen^R) of pRL662-GFP(S65T) (Yu *et al.*, 2021) was
143 replaced by spectinomycin resistance gene from 35S::RUBY to obtain pRL662-
144 GFP(S65T)/Spe^R by use of Gibson Assembly® Master Mix (New England Biolabs,
145 USA). The expression of mCherry2 with a 3'-end nuclear localization signal
146 (mCherry-NLS) was generated from pEB2-2ndVal mCherry2-L (Addgene#104027)
147 by PCR. PCR was performed by use of KAPA HiFi HotStart ReadyMix PCR Kit
148 (KapaBiosystems, South Africa) and PCR products were cloned into the
149 pJet1.2/blunt plasmid following the user manual of CloneJET PCR Cloning Kit
150 (ThermoFisher Scientific, USA). 35S::mCherry2-SV40/Kan^R binary vector was
151 constructed with Golden Gate Assembly.

152 A3A-CBE coding region was amplified from pYPQ265E2 (Addgene #164719) and
153 was subcloned into XbaI/SacI digested pHEE901 (Addgene #91707) via Gibson
154 Assembly. Protospacers were cloned into pA3A-CBE vectors as previously
155 described (Steinert *et al.*, 2015). To generate the *tufAB*$^{Pst4-15}$ mutants in GV3101, we
156 employed double crossover vector using pEML041003-tufAPst4-15 and pEML41003-
157 tufBPst4-15. Two 2.5-kb DNA fragments of modified *tufA* and *tufB* were amplified by
158 two pairs of primers, and cloned into pEML041003 by BsaI digestion. AS201 was
159 generated by modifying *tufB* followed by *tufA*, while AS202 was *tufA* followed by
160 *tufB*. In both constructs, the amino acids at positions 4-15 of EF-Tu were substituted
161 from the native sequence SKFERNKPHVNI to the *Pseudomonas syringae* variant
162 EKFDRSLPHCNV.

163 **Seedling transient transformation and GUS activity assays**

164 *A. thaliana* seedling transient expression assay was performed by the AGROBEST
165 (*Agrobacterium*-mediated enhanced seedling transformation) method as previously
166 described, with minor modification (Wu *et al.*, 2014). *Agrobacterium* cultures were
167 adjusted to an OD_{600}=0.01 in AB-MES medium for co-culture with seedlings. Infected
168 seedlings were collected for GUS activity assays after 2.5 day-post-inoculation.

169 ***Agrobacterium*-mediated transformation by floral inoculation (AMT-FI)**

170 AMT-FI was performed according to the published procedure (Clough & Bent, 1998)
171 with modifications. For tracking *Agrobacterium* cells and transformation events, each
172 *Arabidopsis* plant was grown in a small pot (5 cm upper diameter x 5 cm high x 3.5
173 cm bottom diameter). For genome editing experiments, three plants were grown in a
174 large pot (7.8 cm upper diameter x 7.8 cm high x 5.7 cm bottom diameter). Plants
175 were grown until they reached ~5 weeks old, with primary inflorescences reaching
176 10 to 15 cm tall. The primary inflorescence was then removed to promote the
177 emergence of secondary inflorescences over the next 5 to 6 days. Immediately prior
178 to floral dipping, all open flowers were removed. Inflorescences were submerged in
179 *Agrobacterium*-containing infiltration medium for 40 seconds, then plants were laid
180 horizontally in trays, covered with plastic film to maintain high humidity, kept in the
181 dark and incubated for 20 to 24 hrs. Plants were returned to the growth room under
182 the same growth condition.

183 For time-course experiments, newly opened flowers were labeled daily following
184 inoculation. GFP-labeled *Agrobacterium* cells and mCherry2 T-DNA reporter signals
185 were examined in ovaries using a Zeiss LSM 510 Meta confocal microscope

186 RUBY signals were monitored visually in plants transformed with GV3101 carrying
187 the 35S::RUBY construct, assisted by a stereo microscope. A Zeiss Lumar V12
188 stereo fluorescent microscope was used to capture images of floral organs,
189 developing ovules, seeds, and seedlings.

190 To evaluate AMT-FI efficiency by RUBY marker, siliques from RUBY-transformed
191 plants were collected daily. To assess stable transformation efficiency, seeds were
192 sterilized in 70% ethanol for 10 min and plated on a 1/2 MS medium supplemented
193 with 25 mg/L hygromycin. The number of germinated seedlings and Hyg^R seedlings
194 was recorded. AMT-FI efficiency was determined based on the proportion of Hyg^R
195 seedlings relative to the total number of germinated seedlings.

196 **Assessment of genome editing efficiency**

197 To simultaneously measure the genome editing and AMT-FI efficiency, seeds from
198 plants transformed with *Agrobacterium* carrying a binary vector with T-DNA-encoded
199 base editor, a sgRNA and a hygromycin resistance gene were surface sterilized and
200 germinated on a 1/2 MS medium supplemented with either 5 mg/L tribenuron or 25
201 mg/L hygromycin, both containing 100 mg/L timentin. After seven days, the numbers
202 of tribenuron-resistant, hygromycin-resistant, and albino T1 seedlings were recorded.
203 AMT-FI efficiency was estimated using a weight-based approach, with 10 mg of
204 seeds estimated to contain approximately 500 seeds.

205 **Statistical analysis**

206 An unpaired two-tailed Student's *t*-test, performed using GraphPad Prism 10, was
207 used to assess statistical differences either between Col-0 WT and *efr* mutants or
208 across time-course datasets.

209

210 **RESULTS**

211 ***Agrobacterium* enters the female reproductive organ within one hour but**
212 **transformation events occur in open flowers after five day-post inoculation**

Although transformation is thought to occur when the female gametophyte becomes accessible, direct links between floral stage and transformation success remain unclear. To investigate the spatial and temporal dynamics of *Agrobacterium* infection and transformation, we engineered a fluorescently labeled *Agrobacterium* strain for live tracking. *Agrobacterium* GV3101 carrying the disarmed Ti plasmid pMP90 (hereafter referred as GV3101), constitutively expressing GFP marker and a T-DNA expressed mCherry2, was used for floral inoculation in *A. thaliana* Col-0 (Fig.1a, 1b). GFP-expressing *Agrobacterium* cells were observed as early as 1 hour-post-inoculation (HPI) in the early developmental stage of open gynoecia, the female reproductive organ lacking central placenta tissue (Fig. 1c) but were not detected in the later stage of gynoecia containing central placenta tissue (Fig. 1d). This implied that developing placenta may act as a physical barrier to *Agrobacterium* entry during early infection. By 6 HPI, *Agrobacterium* cells accumulated in the locule of open gynoecia (Fig. 1e, 1f), whereas no signal was seen in closed gynoecia (Fig. 1g). This indicated that open gynoecia serve as the main entry point of *Agrobacterium* into the locule before development of female gametophyte.

At one day-post-inoculation (DPI), *Agrobacterium* cells were detected in locules of younger gynoecia (Figs. 1h, S1a-f) but were absent in older gynoecia undergoing ovule development (Figs. 1i, S1g-n). Among more than 30 gynoecia examined, all 13 open gynoecia observed at 6 HPI and 1 DPI showed detectable GFP signals in the locule, indicating the entrance of *Agrobacterium* prior to the closure of gynoecia. At 3 DPI, *Agrobacterium* persisted in the locules of more mature gynoecia (Fig. 1j), and at 5 DPI, just prior to floral opening (anthesis), *Agrobacterium* cells were enriched around the micropyles, the ovular opening through which the pollen tube and possibly *Agrobacterium* gain access (Fig. 1k). Despite the sustained presence of *Agrobacterium*, successful T-DNA expression indicated by mCherry2 fluorescence was not detected before anthesis (Fig. 1c-k). Similarly, the RUBY reporter signal was absent in gynoecial tissues until after flower opening (Fig. 2c). Following anthesis, mCherry2 signals became visible in cells adjacent to the egg cell/zygote and in the micropyle region where *Agrobacterium* cells had accumulated (Fig. 1l, 1m). Transformation signals were also detected in the integument, the ovule's outer protective layer (Fig. 1m).

Together, these observations reveal that while *Agrobacterium* rapidly enters the open gynoecium as early as 1 HPI, transformation events are temporally restricted, becoming detectable only in flowers that opened from 5 DPI onward. This correlates with key developmental transitions in ovule accessibility and gametophyte maturity.

RUBY-based reporter system uncovers transformation dynamics and floral abnormalities

The current method for quantifying transformation efficiency of AMT-FI primarily relies on the use of antibiotic resistance genes, using survival rates of T1 seedlings as a proxy for transformation efficiency. However, this approach overlooks transient transformation events that occur at early stages post-inoculation. To better capture both the transient and stable transformation events, we developed a dual-reporter system combining the visible RUBY marker with a hygromycin-resistance gene (Fig. 3a).

We first assessed the floral organs exhibiting RUBY expression. The earliest detection of RUBY signals was observed at 4 DPI, localized at the sepals of floral buds (Fig. 2a). By 5 DPI, RUBY expression appeared on the stigma of open flowers but not on pollen grains (Fig. 2b). Dissection of the ovaries revealed RUBY signal in the transmitting tissues (Fig. 2c), as well as in ovules and developing seeds (Fig. 2d, 2e). While many RUBY ovules were abortive (Fig. 2d), others continued to develop normally (Fig. 2e). Most flowers developed and opened normally (Fig. 2f) while a minor subset exhibited developmental abnormalities. These included flowers with partially open petals (Fig. 2g) and those where only the gynoecium emerged from the sepals (Fig. 2h). In mature seeds, RUBY expression ranged in intensity from light pink to dark purple (Fig. 2i), indicating variable expression levels.

In the hygromycin resistance assay, most Hyg^R seedlings only showed weak or sparse RUBY signals, with ~10% or less of T1 seedling showing RUBY in whole seedlings (Fig. S2). Because hygromycin-sensitive seedlings can continue to grow for up to seven days before growth arrest due to their inability to form roots on hygromycin-containing medium, we can still observe $RUBY^+/Hyg^S$ seedlings, although their frequency is low (less than 1% of total transformants, Fig. 2j). Consequently, not all hygromycin-resistant plants exhibited uniform RUBY expression throughout the plants (Fig. 2k). Overall, the percentage of RUBY-positive

277 seeds was higher than the frequency of Hyg^R seedlings. This discrepancy may
278 reflect transient expression or expression of RUBY marker in the integument, which
279 does not necessarily indicate stable T1 transformation.

280 Collectively, the dual-reporter system offers a more comprehensive and sensitive
281 tool for monitoring transformation events across the reproductive tissues. The RUBY
282 reporter revealed that AMT-FI enables transformation in a variety of tissues within
283 the female reproductive organ. However, it also uncovered associated
284 developmental abnormalities in flowers and ovules, which in some cases prevent
285 transformed ovules from developing into viable seeds.

286 **_Agrobacterium_ infection and EFR-mediated immunity synergistically disrupt**
287 **ovule development and seed viability**

288 Since transformation events were only observed in ovaries after anthesis, we sought
289 to trace the occurrence of AMT events in developing siliques using RUBY reporter as
290 a marker (Fig. 3a). Flowers that opened between 1 to 10 DPI were labeled daily.
291 Once embryos were fully developed, approximately 10 days after floral opening and
292 pollination (Baud *et al.*, 2002), each corresponding silique was examined for RUBY
293 signals in ovules/developing seeds.

294 To assess the impact of EFR-mediated immunity on AMT-FI efficiency, we compared
295 transformation efficiency in Col-0 wild-type (WT) plants and two *EFR* loss-of-function
296 mutants (*efr*-1 and *efr*-2) (Zipfel et al., 2006). Transformation events were primarily
297 detected in flowers that opened between 5 to 9 DPI, with the highest frequency,
298 nearly 100% of siliques showing RUBY-positive ovules in flowers opened at 6 DPI in
299 both Col-0 WT and *efr* mutants (Fig. 3b). The percentage of siliques harboring RUBY
300 ovules did not differ significantly between WT and *efr*, suggesting that *Agrobacterium*
301 can access the open gynoecium and subsequently transform ovules with
302 comparable success across genotypes. However, the proportion of RUBY-positive
303 ovules per silique was moderately higher in *efr* mutants, suggesting that
304 compromising EFR-mediated PTI can enhance transformation efficiencies (Figs. 3c,
305 S3a, S3b). Importantly, the number of siliques per plant and total seed number did
306 not show significant difference between WT and *efr* mutants (Fig. S4). Thus, the
307 higher RUBY transformation rate per silique in *efr* mutants (Figs. 3c, S3b) is not
308 caused by variation of siliques or seeds between Col-0 and *efr* mutant plants.

309 Given that AMT-FI often induced floral abnormalities and ovule abortion, we further
310 investigated whether EFR-mediated PTI affects ovule viability. Strikingly, in Col-0
311 WT, nearly 60% of RUBY-positive ovules were abortive, indicating a strong negative
312 impact of AMT-FI on ovule development. In *efr* mutants, although ovule abortion still
313 occurred, the rate was significantly reduced to ~45%. In contrast, fewer than 20% of
314 non-RUBY ovules were abortive, with no significant difference between Col-0 WT
315 and *efr* mutants (Fig. 3d). On average, *Agrobacterium* infection resulted in an ovule
316 abortive rate of ~35% (Figs. 3d, S3c).

317 Notably, a strong negative correlation was observed between transformation rate
318 and seed viability. Flowers that opened at 6 DPI, despite showing the highest AMT-
319 FI efficiency, produced low number of viable seeds (Fig. 4a), likely due to the high
320 abortion rate of RUBY-positive ovules (Fig. 3d). However, *efr* mutants produced
321 significantly more viable seeds per silique than Col-0 WT from flowers that opened at
322 6 to 8 DPI (Fig. 4a), supporting a role for EFR-mediated immunity in transformation-
323 associated ovule abortion.

324 To determine whether the increased number of viable seeds per silique in *efr*
325 mutants is a consequence of AMT-FI, we quantified seed production in plants treated
326 with infiltration medium, and those inoculated with *Agrobacterium* GV3101 (Fig. S5).
327 Under both conditions, *efr* mutants produced more seeds per silique than Col-0 WT
328 (Fig. S5a, S5b). However, *Agrobacterium* infection further reduced seed numbers in
329 both genotypes. To assess seed viability, we evaluated germination rates. Seeds
330 from plants treated with infiltration medium germinated at nearly 100% but the
331 germination rate is reduced in both Col-0 and *efr* (~90%) with *Agrobacterium*
332 infection. However, when the number of developed/germinated seeds following
333 *Agrobacterium* infection is normalized to that of seeds treated with infiltration
334 medium, *efr* mutants exhibited higher seed development and germination rates (Fig.
335 S5a).

336 Taken together, the results suggested that the elevated abortion rates and reduced
337 seed viability observed here are largely attributable to *Agrobacterium* infection
338 because ovule abortion rates are typically less than 1% under normal growth
339 conditions (van Tol *et al.*, 2022). EFR-mediated immunity may also reduce seed
340 development and viability but pathogen-induced stress from *Agrobacterium* infection
341 has a more substantial negative impact than through EFR alone. While alleviation of

342 EFR-mediated immunity reduced the abortion rate among transformed ovules by
343 ~15%, it did not restore ovule viability to levels observed in non-transformed ovules
344 (Fig. 3d). These findings suggest that, in addition to EF-Tu PAMP recognition, other
345 *Agrobacterium*-derived factors likely contribute to ovule developmental disruption
346 during AMT-FI.

347 **Temporal profiling reveals the optimal window for stable AMT-FI**
348 **transformation**

349 Although the RUBY-positive ovules and seeds indicate transformation events, not all
350 develop into viable transgenic T1 seeds. To more accurately evaluate inherited
351 transformation efficiency, we quantified the number of viable transgenic seeds per
352 silique and stable transformation rate using hygromycin resistance as a selection
353 marker. Stable transformation efficiency was calculated based on the number and
354 percentage of Hyg^R seedlings collected daily from flowers opened at 5-9 DPI (Figs.
355 4, S4c).

356 As expected, siliques from flowers opened at 6 DPI exhibited the highest
357 transformation efficiency, with an average of ~90% and a peak at 100% of siliques
358 containing one or multiple Hyg^R transformants (Fig. 4b). Consistently, stable
359 transformation efficiency peaked at this time point, with an average of ~26% and a
360 peak at 40% of T1 progeny exhibiting hygromycin resistance (Fig. 4c). The number
361 of T1 Hyg^R transformants per plant also reached its highest at 6 DPI, averaging ~55
362 and peaking at 100 per plant (Fig. 4d).

363 These results highlight that flowers opened at 6 DPI as the optimal floral stage for
364 achieving the highest frequency of stable AMT-FI-mediated transformation in
365 *Arabidopsis*.

366 **EFR-mediated immunity suppresses genome editing efficiency**

367 Notably, no significant increase in stable transformation efficiency was observed in
368 *efr* mutants compared to Col-0 WT (Fig. 4c), similar to the previous findings (van Tol
369 *et al.*, 2022; Yang et al., 2023). Previous studies have shown that *efr* mutants exhibit
370 enhanced *Agrobacterium*-mediated transient expression (Zipfel et al., 2006; Wu, Liu
371 et al., 2014). Since transient expression of CRISPR/Cas9 components is sufficient to
372 induce genome editing without stable T-DNA integration, we next investigated

373 whether EFR-mediated immunity adversely affects gene editing efficiency during
374 AMT-FI.

375 We constructed a T-DNA vector carrying dual selection markers: a hygromycin
376 resistance gene for selecting transgenic plants and a CRISPR/Cas9 system
377 targeting the *ALS* gene, which confers dominant herbicide resistance (Chen *et al.*,
378 2017), for identifying genome-edited plants (Fig. 5a). Given that the egg-cell is a
379 major target of AMT-FI (Desfeux *et al.*, 2000), we adopted a strategy that enables
380 editing in monoploid germline cells at early developmental stages. Specifically, we
381 applied an egg-cell-specific promoter previously shown to induce heritable mutations
382 in the T1 generation (Wang *et al.*, 2015). To enhance genome editing efficiency and
383 streamline the screening process, we employed an A3A/Y130F-CBE_V01 base
384 editor (termed as A3A-CBE in this study), which has demonstrated efficient C-to-T
385 base editing in both rice and *Arabidopsis* under a ubiquitin promoter (Ren *et al.*,
386 2021).

387 Using this construct, we transformed Col-0 WT and *efr* mutants and assessed T1
388 progeny for T-DNA integration (via hygromycin resistance) and genome editing (via
389 tribenuron resistance conferred by *ALS* editing). The A3A-CBE system achieved an
390 overall editing frequency of approximately 0.5% in total T1 seeds (Fig. 5b). Both *efr*-1
391 and *efr*-2 mutants showed higher editing rates, despite the increase being
392 statistically significant only in *efr*-2. We also evaluated stable transformation
393 efficiency by sowing T1 seeds on a hygromycin-containing medium but no significant
394 increase can be observed in *efr* mutants (Fig. 5c).

395 To further validate these findings, we targeted *CLA1* and *PDS3*, two genes that
396 cause albino phenotypes when biallelically edited (Liu *et al.*, 2022). T1 seeds were
397 germinated on a hygromycin-containing medium, and the numbers of green and
398 albino seedlings were quantified (Fig. 5d). We observed a slight but consistent
399 increase in the proportion of albino seedlings in *efr*-1 compared to Col-0 WT,
400 supporting the conclusion that EFR-mediated immunity suppresses genome editing
401 efficiency during AMT-FI.

402 **Modification of *Agrobacterium* EF-Tu enhances transient gene expression and**
403 **genome editing efficiency but not stable T-DNA integration efficiency**

404 To further validate the role of EFR in suppressing genome editing efficiency during
405 AMT-FI, we tested whether an *Agrobacterium* strain that evades EFR recognition
406 mediates increased genome editing efficiency. To achieve this, we engineered
407 *Agrobacterium* to express a modified EF-Tu incapable of triggering EFR-mediated
408 PTI. *Agrobacterium* GV3101 possesses two EF-Tu-encoding genes, *tufA and tufB*,
409 which produce a translation elongation factor. Our initial attempts to delete both *tuf*
410 genes were unsuccessful, likely due to their essential function. However, a recent
411 study demonstrated that replacing the DNA fragment encoding entire or N-terminal
412 region (amino acids 1-15) of *Agrobacterium* EF-Tu with that of *Pseudomonas*
413 *syringae* pv. *tomato* (*Pst*) DC3000 reduced PTI activation and improved transient
414 expression efficiency in *A. thaliana* leaves (Yang *et al.*, 2023).

415 Because the first three amino acids of EF-Tu are identical between GV3101 and *Pst*
416 DC3000, we adopted a similar concept but applied a different experimental strategy
417 to engineer GV3101 by replacing amino acids 4-15 of both *tufA* and *tufB* with the
418 corresponding region from *Pst* EF-Tu, referred to as $tufAB^{Pst4\text{-}15}$ (Fig. 6a). We
419 generated two independent $tufAB^{Pst4\text{-}15}$ strains, named as AS201 and AS202, and
420 compared them to the parental GV3101 strain for transient expression, genome
421 editing and stable transformation efficiencies. To assess transient transformation, we
422 transformed *A. thaliana* seedlings for transient expression analysis using a T-DNA-
423 encoded GUS reporter (Wu *et al.*, 2014). Both AS201 and AS202 showed
424 significantly higher transient GUS activity in Col-0 WT compared to GV3101 (Fig. 6b,
425 6c). As expected, GV3101 exhibited ~20-fold higher GUS activity in *efr*-1 than in Col-
426 0 due to the absence of EF-Tu recognition. However, in *efr*-1*,* AS201 and AS202
427 exhibited lower GUS activity than GV3101, indicating that the engineered EF-Tu
428 proteins may compromise transformation efficiency when PTI is not a barrier for
429 infection.

430 Encouraged by these results, we next tested whether the $tufAB^{Pst4\text{-}15}$ strains could
431 improve genome editing efficiencies in Col-0 by AMT-FI. Compared to GV3101, both
432 AS201 and AS202 significantly enhanced genome editing rates and produced more
433 edited T1 plants (Fig. 6d). As expected, we observed no significant difference in T-
434 DNA integration rates or in the total number of transgenic T1 plants (Fig. 6e).

435 **Sequencing-based screening of genome-edited plants**

436 Our floral inoculation analysis demonstrated that flowers opened at 6 DPI showed a
437 stable transformation efficiency ~26% (Fig. 4c). Based on this high efficiency, we
438 reasoned that it may be possible to recover genome-edited T1 plants without prior
439 selection for the T-DNA marker (Fig. 7a).

440 To test this, we targeted *CLA1* gene, which allows easy identification of edited plants
441 based on their albino phenotype, complemented by sequencing analysis. We
442 germinated T1 seeds from Col-0 and *efr* mutants on MS medium without hygromycin
443 selection. Among these seedlings, we observed biallelically edited albino plants at
444 the frequencies of 3.3% in Col-0, 3.7% in *efr*-1, and 4.2% in *efr*-2. We also identified
445 green seedlings carrying monoallelic edits, identified by Sanger sequencing. Their
446 editing rates were 1.6% in Col-0, 15.9% in *efr*-1, and 4.7% in *efr*-2 (Fig. 7b). To
447 further validate this strategy, we targeted the *ALS* gene without applying tribenuron
448 selection. Among the T1 seedlings, we identified one edited plant out of 94 T1
449 seedlings using GV3101 and two out of 93 using the $tufAB^{Pst4\text{-}15}$ mutant, AS201. All
450 three edited T1 plants carried C-to-T base editing at the Pro197 locus, consistent
451 with the expected *ALS* editing outcome (Fig. 7b).

452 In conclusion, genome-edited T1 plants can be obtained without prior selection for T-
453 DNA integrated plants when screening seeds from flowers opened at 6 DPI.
454 Furthermore, evading EFR-mediated PTI enhances genome editing efficiency,
455 further supporting the role of plant immunity in constraining *Agrobacterium*-based
456 genome engineering.

457

458 **DISCUSSION**

459 In this study, we provide mechanistic and practical insights into the *Agrobacterium*-
460 mediated floral transformation process. By tracking transformation events with a
461 dual-reporter system, we identified the optimal transformation window, leading to the
462 success in obtaining edited plants without prior selection of T-DNA integration. Our
463 findings also reveal EFR-mediated immunity as an important barrier to efficient
464 transient transformation and genome editing via AMT-FI.

465 By integrating floral stage selection, immune evasion, and *Agrobacterium*
466 engineering, our study provides a practical guideline to advance *Agrobacterium*-
467 mediated plant transformation and genome engineering. The recommended AMT-FI

468 procedure is summarized in Fig. S6. First, the engineered *tufAB*-modified strain
469 AS201, which showed relatively better performance than AS202, is recommended to
470 replace GV3101 for plant transformation in *Arabidopsis* or other plants possessing
471 *EFR*. Second, we recommend to collect seeds only from flowers that opened 5~9
472 day-post-inoculation (DPI), which yield 4~5% hygromycin-resistant transformants
473 (Fig. 4c, 5), compared with ~2% when seeds are collected from all flowers (Fig. 6e).
474 Third, for screening edited T1 plants without prior selection for T-DNA integration,
475 collecting seeds exclusively from flowers opened at 6 DPI can reduce labor and cost
476 as well as increase the frequency of obtaining edited plants (Fig. 7). In our
477 experimental condition, it is critical to follow the experimental procedure for growing
478 only one plant in a small pot (5 cm upper diameter × 5 cm height × 3.5 cm bottom
479 diameter). When growing three plants in one larger pot, the peak of AMT-FI
480 efficiency is generally delayed by approximately one day.

481 **Temporal and spatial tracking of *Agrobacterium* entry and transformation**

482 Using RUBY as a T-DNA reporter, we detected strong RUBY signals in sepal,
483 transmitting tissues, ovules, and developing seeds (Fig. 2). Notably, no RUBY
484 signals were detected in pollen grains, consistent with earlier findings using GUS
485 reporter (Ye *et al.*, 1999; Bechtold *et al.*, 2000; Desfeux *et al.*, 2000). The variation in
486 transformation efficiency likely reflects cell-type specific susceptibility to
487 *Agrobacterium* infection or differential transcriptional activity of the CaMV 35S
488 promoter (Kiselev *et al.*, 2021). Additionally, we observed diverse RUBY expression
489 patterns among hygromycin-resistant transgenic plants. Some plants expressed
490 RUBY throughout their life cycle, while others showed expression only during
491 seedling stages or specific organs. This variability may result from positional effects
492 of T-DNA integration site or differences in promoter activity (Gelvin, 2003; Roca
493 Paixao & Deleris, 2024). The presence of hygromycin-sensitive but RUBY-positive
494 seedlings suggests either truncation of the T-DNA at the left border (Fig. 3a), where
495 the hygromycin-resistance cassette is located, or the weaker activity of the *nos*
496 promoter driving expression of the hygromycin-resistance gene.

497 Although various floral tissues and cell types can be transformed (Figs. 1, 2), only
498 female gametes serve as heritable targets for producing progenies in *Arabidopsis*
499 (Ye *et al.*, 1999; Bechtold *et al.*, 2000; Desfeux *et al.*, 2000). Therefore,
500 *Agrobacterium* entry into the locule of developing gynoecium is a crucial step in

501 successful transformation (Desfeux *et al.*, 2000). Our data show that *Agrobacterium*
502 enters the locule of open gynoecium within hours, colonizes reproductive tissues,
503 and persists around the micropyle of ovules, potentially enabling transformation of
504 egg cells and surrounding tissues. Despite early colonization, transformation events
505 in gynoecium cells only occur in open flowers from 5 DPI onward, coinciding with
506 floral opening and micropyle exposure.

507 Transient T-DNA expression can be observed as early as 1 DPI and highly abundant
508 at 2 DPI when transforming somatic cells like leaves, seedlings, and root explants
509 (Gelvin, 2003; Wu *et al.*, 2014; Lopez-Agudelo *et al.*, 2024). The delayed expression
510 in germ cells may reflect differences in promoter activity, cell-type susceptibility, or
511 route of *Agrobacterium* entry. Given that pollen tubes access ovules via the
512 micropyle only after floral opening, they may serve as important carriers, facilitating
513 *Agrobacterium* entry into ovules for transformation. Once inside, *Agrobacterium*
514 could associate with male gametes or directly attach to egg cells for T-DNA transfer
515 during fertilization. This proposed mechanism explains the high AMT-FI efficiency
516 observed in flowers opening at 5-9 DPI and suggests that transformation occurs in
517 young floral buds 5-9 days before anthesis, supporting previous findings (Clough &
518 Bent, 1998; Ye *et al.*, 1999; Desfeux *et al.*, 2000).

519 **AMT peaks in flowers opened at 6 DPI and negatively correlate with seed**
520 **viability**

521 Tracking transformation events by fluorescent marker revealed *Agrobacterium*
522 targets integument cells (Fig. 1l, 1m), consistent with previous findings (Bechtold *et*
523 *al.*, 2003). However, only the transformed egg cells contribute to transgene
524 inheritance. This explains why RUBY-based transformation rates are significantly
525 higher than those determined by hygromycin resistance (Figs. 3c, 4c). The use of the
526 RUBY reporter enabled the discovery of floral stages accessible for AMT-FI,
527 revealing that nearly all ovaries from flowers open at 6 DPI were transformed (Fig.
528 3b), yielding averaged an 26% stable Hyg^R T1 progeny (Fig. 4c). However, high
529 transformation rates were accompanied by increased ovule abortion, resulting in
530 fewer viable seeds (Figs. 3d, 4a, 4c). In contrast, *efr* mutants exhibited lower
531 abortion rates and higher seed viability per silique, suggesting that EFR-triggered
532 immunity contributes to transformation-induced ovule loss. Evading plant immune

533 responses could therefore enhance the efficiency of transgenic seed production via
534 AMT-FI.

535 **Evasion of EFR-mediated immunity enhances genome editing efficiency but**
536 **not stable transformation**

537 Although EFR-mediated immunity was discovered nearly two decades ago (Zipfel *et*
538 *al.*, 2006), its influence on stable transformation and genome editing remain unclear
539 until recent studies. While *efr*-1 mutants showed no improvement on gene targeting
540 or stable transformation efficiencies (van Tol *et al.*, 2022), they do exhibit enhanced
541 transient expression (Zipfel et al., 2006; Wu, Liu et al., 2014; Yang et al., 2023). Our
542 results revealed higher RUBY transformation rates in *efr* ovules, and confirmed no
543 significant increase in stable transformation measured by hygromycin resistance
544 (Figs. 4c, 6e).

545 However, we showed that genome editing efficiencies were higher in *efr* mutants and
546 in Col-0 WT inoculated with the two engineered GV3101::*tufAB*$^{Pst4\text{-}15}$ strain, AS201
547 and AS202 (Figs. 5, 6). This suggests that genome editing can be decoupled from T-
548 DNA integration. This is further supported by evidence that genome-edited plants
549 were successfully obtained from the *teb-5* (*polQ)* mutant, whereas T-DNA integrated
550 plants were not (van Tol *et al.*, 2022). Thus, we proposed that enhancement of
551 editing efficiencies may result from higher transient expression of CRISPR/Cas9 in
552 egg cells in the absence of EFR-triggered immunity. Moreover, because editing can
553 occur without DNA integration (e.g., via ribonucleoprotein delivery), it may serve as a
554 proxy for measuring transgene expression levels in germline cells.

555 **Innovative strategies for enhancing genome editing efficiency**

556 Precision editing is critical for inducing dominant phenotypes by targeting an
557 endogenous gene. However, current methods exhibit low efficiency compared to
558 mutagenesis by Cas9 nuclease (Huang & Puchta, 2021). To overcome these
559 limitations, we used an improved A3A-CBE base editor and achieved a high editing-
560 to-integration ratio (~0.2) (Fig. 5). This construct, together with our optimized
561 screening workflow, enables efficient dissection factors that influence stable
562 transformation and genome editing efficiency in *Arabidopsis*.

563 Several recent studies have introduced innovative approaches to enhance stable
564 transformation and genome editing. These include engineering of *Agrobacterium*

strains to deliver type III secretion system effectors, T-DNA concatenation, and vector copy number manipulation (Raman *et al.*, 2022; Dickinson *et al.*, 2023; Szarzanowicz *et al.*, 2024). Our success in engineering *Agrobacterium* strains with modified EF-Tu to evade EFR recognition, significantly enhanced genome editing efficiency. This reinforces the idea that boosting transient gene expression is a key determinant for successful genome modification via CRISPR/Cas9.

Despite native EFR is specific to Brassicaceae, several non-Brassicaceae crops have been engineered to express EFR for disease resistance (Lu *et al.*, 2015; Schwessinger *et al.*, 2015; Boschi *et al.*, 2017; Kunwar *et al.*, 2018; Piazza *et al.*, 2021). These transgenic plants may show reduced *Agrobacterium*-mediated transformation. Our engineered GV3101::*tufAB*$^{Pst4\text{-}15}$ strains could overcome this limitation. Beyond EF-Tu, other *Agrobacterium*-derived PAMPs such as translation initiation factor IF1, cold-shock protein, and flagellin also trigger PTI via distinct receptors in different species (Saur *et al.*, 2016; Fürst *et al.*, 2020; Fan *et al.*, 2022). This work sets the stage for the development of multi-modified *Agrobacterium* strains with broad compatibility, offering a roadmap to enhance AMT across diverse plant taxa.

AUTHOR CONTRIBUTIONS

M.-S.L, T.-K.H., C.-H. K. and E.-M.L, contributed to the conceptualization of the project. M.-S.L. designed and performed AMT-FI. T.-K.H. designed and performed the genome editing assay. M.-S.L., T.-K.H., Y.-C.W. and S.-C.W. performed experiments and analyzed data. M.-S.L., T.-K.H., and E.-M.L. wrote the initial manuscript. E.-M.L., C.-H. K. and C.-H.W. supervised the project. M.-S.L and T.-K.H contributed equally. All authors reviewed and edited the manuscript.

ACKNOWLEDGEMENTS

The authors acknowledge the members of the Lai, Kuo, and Wu labs for discussion and suggestion. We also thank the technical assistance of Live Cell Imaging Core Lab and Sanger DNA sequencing service provided by Genomic Technology Core located at the Institute of Plant and Microbial Biology, Academia Sinica. The funding

596 was supported by the Academia Sinica Grand Challenge Program (AS-GC-111-L02)
597 to E.-M.L., C.-H. K. and C.-H.W, and the intramural fund of the Institute of Plant and
598 Microbial Biology, Academia Sinica.

599

600 **SUPPORTING INFORMATION**

601 Table S1. Plasmid information

602 Table S2. Primer list

603 Figures S1-S6

604

605 **DATA AVAILABILITY**

606 The data supporting the findings of this study are available within the article or as
607 Supporting Information. Strains and plasmids generated in this study are available
608 either on Addgene (no. 234350-234353, 237864-237866) or upon request (Table
609 S1)

610

611 **CONFLICT OF INTEREST STATEMENT**

612 The authors declare no conflict of interest.

613

614 **FIGURE LEGENDS**

615

616 **Figure 1. *Agrobacterium* enter open gynoecium within 1 hour but**
617 **transformation events occur in open flowers after 5 day-post inoculation**

618 (a) *Agrobacterium* GV3101 carrying pRL662-GFP(S65T)/Spe^R and the binary vector
619 35S::mCherry2-NLS was used for floral inoculation on *Arabidopsis thaliana* Col-0 to
620 visualize *Agrobacterium* localization and transformation events.

621 (b) Schematic illustration of the structure and development of gynoecium from early
622 to mature stage with stigma, style, ovary containing ovules. The floral stages and
623 their corresponding durations were indicated according to Smyth et al. The diagram
624 was created with BioRender.com.

625 After one hour-post-inoculation (HPI), *Agrobacterium* cells had already entered the
626 locule of developing gynoecium (c) but were absent in later-stage gynoecia
627 containing developed placenta tissue (d). Between 6-9 HPI, more *Agrobacterium*
628 cells were observed in the locule (e), even at it began to close (f). *Agrobacterium*
629 was not detected in fully closed gynoecia (g).

630 At one day-post-inoculation (DPI), *Agrobacterium* cells were detected in young
631 closed ovaries (h) but not in older ovaries undergoing ovule development (i). At 3
632 DPI (j), *Agrobacterium* cells persisted in ovaries at late developmental stages. By 5
633 DPI, *Agrobacterium* cells were enriched around the micropyle (arrow) (k), though no
634 mCherry2 signal was detected. At floral open stage after 6 DPI, *Agrobacterium*
635 accumulated around the micropyle, and mCherry2 signal became visible (l and m).

636 Asterisks (*) indicate placenta tissue; arrowheads denote developing ovule; arrows
637 indicate *Agrobacterium* located around micropyle. Panels (a to k) were merged
638 channel images; panels (l and m) show GFP, mCherry2, DIC and merged views.
639 Scale bar= 100 μm.

640 **Figure 2. RUBY marker revealed transformation events in floral organs and**
641 **female tissues**

642 RUBY signals were observed in flowers (a), specifically on the stigma but not on
643 pollen grains (b), and in the transmitting tissue (c). In siliques, RUBY expression was
644 detected in both abortive (d) and developing ovules (e).

645 Flower morphology after AMT-FI ranged from normal open flowers (f) to partially
646 open flowers (g), and flowers with only gynoecia emerging from sepals (h).

647 RUBY signal intensity varied among seeds (i) and plants (j, k). (j) At the seedling
648 stage, hygromycin-resistant (Hyg^R) and RUBY-positive seedling (left), non-transgenic
649 seedling (middle), and RUBY-positive but hygromycin sensitive (Hyg^S) seedling
650 (right) were observed. (k) Transgenic T1 plants with variable RUBY expression
651 patterns from strong whole-plant expression to undetectable signal. Scale bar = 200
652 μm.

653 **Figure 3. *Agrobacterium* infection and EFR-mediated immunity exert negative**
654 **impacts on ovule development**

655 (a) Experimental design: a schematic diagram illustrates the 35S::RUBY construct
656 and experimental workflow. Transformation efficiency was evaluated based on the
657 presence of RUBY-positive ovules and hygromycin-resistant seedlings. The diagram
658 was created with BioRender.com.

659 (b) Percentage of siliques with RUBY-positive ovules recorded daily for Col-0 WT,
660 *efr*-1, and *efr*-2 from flowers that opened at 1-10 DPI. Data are mean ± SD of three
661 biological replicates from two independent experiments.

662 (c) RUBY-based transformation. Percentage of RUBY-positive ovules (include both
663 developed and abortive ovules) per silique collected from flowers of Col-0 WT, *efr*-1
664 and *efr*-2 opened at 5-9 DPI was calculated (all data points shown in Fig. S3a). Data
665 are mean ± SD of average percentage of RUBY-positive ovules from three
666 independent experiments (circle, triangle and rhombus symbols). Statistically
667 significant differences ($p < 0.05$) between Col-0 WT and *efr* mutants are indicated.

668 (d) Ovule abortion rate. The abortion rate of RUBY-positive, non-RUBY, and total
669 ovules per silique collected from flowers of Col-0 WT, *efr*-1 and *efr*-2 opened at 5-9
670 DPI was calculated (all data points shown in Fig. S3c). Data are mean ± SD of
671 average abortion rate from three independent experiments (circle, triangle and
672 rhombus symbols). Statistically significant differences ($p < 0.05$) between Col-0 WT
673 and *efr* mutants are indicated.

674 **Figure 4. AMT events occur mainly in flowers opened at 5-9 DPI, peaking at 6**
675 **DPI**

676 Siliques and seeds developed from flowers that opened at 5-9 DPI in Col-0 WT, *efr*-1
677 and *efr*-2 mutants were analyzed through viability (a) and hygromycin resistance
678 (Hyg^R) screening (b, c, d) and viability (d). Data are (a) average number of viable
679 seeds per silique, (b) percentage of siliques containing Hyg^R transformants, (c)
680 percentage of Hyg^R transformants and (d) number of Hyg^R transformants per plant.
681 Data are mean ± SD of six biological replicates from two independent experiments
682 (circle and triangle symbols). Statistically significant differences ($p < 0.05$) between
683 Col-0 WT and *efr* mutants are indicated.

684 **Figure 5. EFR suppresses genome editing efficiency**

685 *Agrobacterium* GV3101 carrying a binary vector encoding a base editor and a
686 sgRNA was used for floral inoculation in Col-0 WT and *efr* mutants to assess
687 genome editing and stable transformation efficiencies.

688 (a) A schematic diagram of the binary vector structure for base editing and target
689 gene information.

690 (b) Genome editing efficiency assessed by tribenuron-resistant T1 plants with
691 targeting the *ALS* Pro197 locus.

692 (c) Stable transformation efficiency evaluated by hygromycin resistance.

693 (b) and (c): Seeds are collected from flowers that opened at 5-9 DPI. Each data point
694 represents biological replicates from six independent experiments. Data are mean ±
695 SD, with *p*-values calculated by Student's t-test between Col-0 WT and *efr* mutants.

696 (d) Genome editing efficiency assessed based on albino phenotype in T1 plants,
697 resulting from by loss-of-function mutations at locus *CLA1 and PDS3.* Statistically
698 significant differences between Col-0 WT and *efr* are indicated (*$p < 0.05$, **$p < 0.01$,
699 chi-square analysis).

700 **Figure 6. Modification of *Agrobacterium* EF-Tu enhances transient gene**
701 **expression and genome editing efficiency but not stable T-DNA integration**
702 **efficiency**

703 The two engineered *Agrobacterium tufAB*$^{Pst4\text{-}15}$ strains, AS201 and AS202, were
704 assessed for its efficiency in transient expression, genome editing, and stable
705 transformation in comparison to the parental *Agrobacterium* GV3101.

706 (a) A schematic diagram illustrating the difference of *tufAB* sequences at amino
707 acids 4th to 15th between *Agrobacterium* GV3101 and *Pseudomonas syringae* (*Pst*).

708 (b, c) Comparison of transient transformation efficiencies between the GV3101 WT
709 and two *tufAB*$^{Pst4\text{-}15}$ strains (AS201 and AS202) in *A. thaliana* seedlings by
710 quantitative GUS activity (b) GUS staining (c, scale bar =1 cm). Results are
711 representative of three independent experiments.

712 (d) Comparison of genome editing efficiency between the GV3101 WT and two
713 *tufAB*$^{Pst4\text{-}15}$ strains (AS201 and AS202) measured by the percentage of tribenuron-
714 resistant T1 plants (left) and number of edited T1 plants per three T0 plants (right).

715 (e) Comparison of stable transformation efficiency by the number of hygromycin-
716 resistant T1 plants per three T0 plants, with no significant differences between WT
717 GV3101 and the two *tufAB*$^{Pst4\text{-}15}$ strains (AS201 and AS202).

718 Seeds were collected from all flowers. Each data point represents biological
719 replicates from three independent experiments. All values are shown as mean ± SD,
720 with *p*-values calculated by Student's t-test.

721 **Figure 7. Sequencing-based screening of genome-edited plants**

722 (a) Workflow for screening genome-edited T1 plants from flowers that opened at 6
723 DPI. Seeds were germinated in 1/2 MS medium with only supplemented with
724 timentin to suppress *Agrobacterium* growth without hygromycin selection. 10-day-old
725 T1 plants were analyzed by Sanger sequencing at the *ALS* or *CLA1* loci. The
726 diagram was created with BioRender.com.

727 (b) The number of sequenced T1 plants and editing rates. †indicates the C to T
728 editing at Pro197 locus conferring tribenuron resistance. Statistically significant
729 differences in genome editing (GE) rates between *efr*-1 and WT Col-0 are indicated
730 (*$p < 0.001$, chi-square analysis).

731 **Figure S1. Basipetal analysis of *Agrobacterium* distribution along *Arabidopsis***
732 **inflorescence at 1 DPI.**

733 A basipetal series of flowers from the inflorescence tip (a) to the first open flower at
734 the base (m and n) were dissected to visualize distribution of *Agrobacterium*
735 expressing GFP reporter at 1 DPI. The order was determined in considering the
736 position and developmental stage of flowers. Each figure consists of four imaging

737 channels (o). Scale bars indicated 50 μm. Panels a-e show open gynoecia, f-n are
738 closed gynoecia, m and n are from different regions of the same flower.

739 **Figure S2. Number and percentage of $Hyg^R/RUBY^+$ seedlings.**

740 (a) Representative photo of T1 seedlings screening on hygromycin containing 1/2
741 MS plate. The hygromycin-resistant T1 exhibiting RUBY signals of whole seedling
742 ($Hyg^R/RUBY^+$) was indicated, among the hygromycin-resistant green and larger T1
743 seedling ($Hyg^R/RUBY^-$), and hygromycin-sensitive green but small seedlings
744 ($Hyg^S/RUBY^-$). The hygromycin-sensitive T1 seedlings with RUBY signals
745 ($Hyg^S/RUBY^+$) shown in Fig. 2j are rarely occurred and not present in this photo.

746 (b) Number and percentage of $Hyg^R/RUBY^+$ T1 seedlings in Col-0 WT and *efr*
747 mutants. Total number of Hyg^R T1 seedlings (Total) and those exhibiting RUBY
748 signals of whole seedling ($RUBY^+$) was indicated and the percentage of $Hyg^R/RUBY^+$
749 T1s among total Hyg^R T1s.

750 **Figure S3. EFR-mediated immunity exerts negative impacts on ovule**
751 **development and RUBY-based transformation rate**

752 GV3101 carrying the 35S::RUBY construct was used for AMT-FI to assess RUBY-
753 based transformation efficiency and ovule abortion rate in Col-0 WT and *efr* mutants.
754 Siliques from flowers that opened at 5-9 DPI were analyzed to count the total
755 number of ovules, the number of developed ovules with or without RUBY signals,
756 and the number of abortive ovules with or without RUBY signals per silique.

757 (a) Daily RUBY-based transformation rate per silique. The percentage of RUBY-
758 positive ovules (including both developed and abortive ovules) per silique was
759 calculate at each DPI, as well as cumulatively across 5-9 DPI. Each data point
760 represents the percentage of RUBY-positive ovules per silique.

761 (b) Daily RUBY-based transformation rate of developed ovules per silique. The
762 percentage of RUBY-positive developed (non-abortive) ovules per silique was
763 measured at each DPI, as well as cumulatively across 5-9 DPIs. Each data point
764 represents the percentage of RUBY-positive developed ovules per silique.

765 (c) Daily ovule abortion rate per silique. The percentage of abortive ovules (including
766 both RUBY-positive and RUBY-negative) per silique was recorded at each DPI and

767 cumulatively across 5-9 DPI. Each data point represents the percentage of abortive
768 ovules per silique.

769 Data are shown in mean ± SD from three independent experiments, with *p*-values
770 calculated by Student's t-test between Col-0 WT and *efr* mutants.

771 Related to Figure 3.

772 **Figure S4. Number of siliques, seeds, and hygromycin-resistant seedlings in**
773 **Col-0 WT, *efr*-1 and *efr*-2 mutants after AMT-FI**

774 Siliques and seeds developed from flowers that opened at 5-9 DPI in Col-0 WT, *efr*-1
775 and *efr*-2 mutants were analyzed through number of siliques (a) and seeds (b) per
776 plant, and averaged number of hygromycin-resistant (Hyg^R) seedlings per silique (c).
777 Data are mean ± SD of six biological replicates from two independent experiments
778 (circle and triangle symbols).

779 **Figure S5. *Agrobacterium* infection and EFR-mediated immunity affect seed**
780 **outputs.**

781 (a) Table showing seed number per silique from plants treated with infiltration
782 medium alone or with *Agrobacterium.* Percentage of developed/germinated seeds
783 after infection was normalized to those from infiltration medium (IM) treatment. The
784 resulting percentage of developed and germinated seeds indicated the impact on
785 seed viability.
786 (b) Seed counts and germination rates following IM alone or with *Agrobacterium* IM
787 (IM + GV3101) treatments. Siliques were collected from flowers that opened at 5–9
788 DPI. The total number of seeds and the number of germinated seeds were
789 compared between treatments.
790 Data were collected from two plants per genotype, except for *efr*-1 infected with
791 GV3101, where data were obtained from one plant. Data are shown as mean ± SD,
792 with *p*-values calculated using Student's *t*-test to compare Col-0 WT and *efr* mutants.
793

794 **Figure S6. The recommended AMT-FI procedure.**

795 The experimental procedures for achieving higher AMT-FI efficiency and for
796 screening genome-edited T1 plants without prior selection for T-DNA integration are

797 illustrated. The engineered *tufAB*-modified strain AS201 is recommended for plant
798 transformation in *A. thaliana* or other plant species possessing *EFR*. The optimized
799 transformation window was determined under the growth conditions of *A. thaliana*,
800 with each plant cultivated in a small pot (5 cm upper diameter × 5 cm height × 3.5 cm
801 bottom diameter). The diagram was created with BioRender.com.

802

803

REFERENCES

Anand A, Uppalapati SR, Ryu CM, Allen SN, Kang L, Tang Y, Mysore KS. 2008. Salicylic acid and systemic acquired resistance play a role in attenuating crown gall disease caused by *Agrobacterium tumefaciens*. *Plant Physiol.* **146**(2): 703-715.

Angulo J, Astin CP, Bauer O, Blash KJ, Bowen NM, Chukwudinma NJ, DiNofrio AS, Faletti DO, Ghulam AM, Gusinde-Duffy CM, et al. 2023. CRISPR/Cas9 mutagenesis of the *Arabidopsis* GROWTH-REGULATING FACTOR (GRF) gene family. *Front. Genome Ed.* **5**: 1251557.

Baud S, Boutin J-P, Miquel M, Lepiniec L, Rochat C. 2002. An integrated overview of seed development in *Arabidopsis thaliana* ecotype WS. *Plant Physiol. Biochem.* **40**(2): 151-160.

Bechtold N, Jaudeau B, Jolivet S, Maba B, Vezon D, Voisin R, Pelletier G. 2000. The maternal chromosome set is the target of the T-DNA in the in planta transformation of *Arabidopsis thaliana*. *Genetics* **155**(4): 1875-1887.

Bechtold N, Jolivet S, Voisin R, Pelletier G. 2003. The endosperm and the embryo of *Arabidopsis thaliana* are independently transformed through infiltration by *Agrobacterium tumefaciens*. *Transgenic Res.* **12**(4): 509-517.

Bélanger JG, Copley TR, Hoyos-Villegas V, Charron JB, O'Donoughue L. 2024. A comprehensive review of in planta stable transformation strategies. *Plant Methods* **20**(1): 79.

Bevan M. 1984. Binary *Agrobacterium* vectors for plant transformation. *Nucleic Acids Res.* **12**(22): 8711-8721.

Boschi F, Schvartzman C, Murchio S, Ferreira V, Siri MI, Galván GA, Smoker M, Stransfeld L, Zipfel C, Vilaró FL, et al. 2017. Enhanced bacterial wilt resistance in potato through expression of *Arabidopsis* EFR and introgression of quantitative resistance from *Solanum commersonii*. *Front. Plant Sci.* **8**: 1642.

Chen Y, Wang Z, Ni H, Xu Y, Chen Q, Jiang L. 2017. CRISPR/Cas9-mediated base-editing system efficiently generates gain-of-function mutations in *Arabidopsis*. *Sci. China Life Sci.* **60**(5): 520-523.

Clough SJ, Bent AF. 1998. Floral dip: a simplified method for *Agrobacterium*-mediated transformation of *Arabidopsis thaliana*. *Plant J.* **16**(6): 735-743.

Desfeux C, Clough SJ, Bent AF. 2000. Female reproductive tissues are the primary target of *Agrobacterium*-mediated transformation by the *Arabidopsis* floral-dip method. *Plant Physiol.* **123**(3): 895-904.

Dickinson L, Yuan W, LeBlanc C, Thomson G, Wang S, Jacob Y. 2023. Regulation of gene editing using T-DNA concatenation. *Nat. Plants* **9**(9): 1398-1408.

Dodds PN, Chen J, Outram MA. 2024. Pathogen perception and signaling in plant immunity. *Plant Cell* **36**(5): 1465-1481.

Fan L, Fröhlich K, Melzer E, Pruitt RN, Albert I, Zhang L, Joe A, Hua C, Song Y, Albert M, et al. 2022. Genotyping-by-sequencing-based identification of *Arabidopsis* pattern recognition receptor RLP32 recognizing proteobacterial translation initiation factor IF1. *Nat. Commun.* **13**(1): 1294.

Fürst U, Zeng Y, Albert M, Witte AK, Fliegmann J, Felix G. 2020. Perception of *Agrobacterium tumefaciens* flagellin by FLS2(XL) confers resistance to crown gall disease. *Nat. Plants* **6**(1): 22-27.

Gelvin SB. 2003. *Agrobacterium*-mediated plant transformation: the biology behind the "gene-jockeying" tool. *Microbiol. Mol. Biol. Rev.* **67**(1): 16-37, table of contents.

Hooykaas PJJ. 2023. The Ti plasmid, driver of *Agrobacterium* pathogenesis. *Phytopathology* **113**(4): 594-604.

Huang T-K, Puchta H. 2021. Novel CRISPR/Cas applications in plants: from prime editing to chromosome engineering. *Transgenic Res.* **30**(4): 529-549.

Hwang HH, Yu M, Lai EM. 2017. *Agrobacterium*-mediated plant transformation: biology and applications. *Arabidopsis Book* **15**: e0186.

854 **Kado CI, Heskett MG. 1970.** Selective media for isolation of *Agrobacterium*, *Corynebacterium*,
855 *Erwinia*, *Pseudomonas*, and *Xanthomonas*. *Phytopathology* **60**(6): 969-976.
856 **Kiselev KV, Aleynova OA, Ogneva ZV, Suprun AR, Dubrovina AS. 2021.** 35S promoter-driven
857 transgenes are variably expressed in different organs of *Arabidopsis thaliana* and in
858 response to abiotic stress. *Mol. Biol. Rep.* **48**(3): 2235-2241.
859 **Kunwar S, Iriarte F, Fan Q, Evaristo da Silva E, Ritchie L, Nguyen NS, Freeman JH, Stall RE, Jones JB,**
860 **Minsavage GV, et al. 2018.** Transgenic expression of EFR and Bs2 genes for field
861 management of bacterial wilt and bacterial spot of Tomato. *Phytopathology* **108**(12): 1402-
862 1411.
863 **Lacroix B, Citovsky V. 2019.** Pathways of DNA transfer to plants from *Agrobacterium tumefaciens*
864 and related bacterial species. *Annu. Rev. Phytopathol.* **57**: 231-251.
865 **Liu D, Xuan S, Prichard LE, Donahue LI, Pan C, Nagalakshmi U, Ellison EE, Starker CG, Dinesh-Kumar**
866 **SP, Qi Y, et al. 2022.** Heritable base-editing in *Arabidopsis* using RNA viral vectors. *Plant*
867 *Physiol.* **189**(4): 1920-1924.
868 **Lopez-Agudelo JC, Goh F-J, Tchabashvili S, Huang Y-S, Huang C-Y, Lee K-T, Wang Y-C, Wu Y, Chang**
869 **H-X, Kuo C-H, et al. 2024.** *Rhizobium rhizogenes* A4-derived strains mediate hyper-efficient
870 transient gene expression in *Nicotiana benthamiana* and other solanaceous plants. *Plant*
871 *Biotechnol. J.*
872 **Lu F, Wang H, Wang S, Jiang W, Shan C, Li B, Yang J, Zhang S, Sun W. 2015.** Enhancement of innate
873 immune system in monocot rice by transferring the dicotyledonous elongation factor Tu
874 receptor EFR. *J. Integr. Plant Biol.* **57**(7): 641-652.
875 **Mysore KS, Kumar CT, Gelvin SB. 2000.** *Arabidopsis* ecotypes and mutants that are recalcitrant to
876 *Agrobacterium* root transformation are susceptible to germ-line transformation. *Plant J.*
877 **21**(1): 9-16.
878 **Nam J, Matthysse AG, Gelvin SB. 1997.** Differences in susceptibility of *Arabidopsis* ecotypes to
879 crown gall disease may result from a deficiency in T-DNA integration. *Plant Cell* **9**(3): 317-
880 333.
881 **Nishizawa-Yokoi A, Saika H, Hara N, Lee LY, Toki S, Gelvin SB. 2021.** *Agrobacterium* T-DNA
882 integration in somatic cells does not require the activity of DNA polymerase θ. *New Phytol.*
883 **229**(5): 2859-2872.
884 **Piazza S, Campa M, Pompili V, Costa LD, Salvagnin U, Nekrasov V, Zipfel C, Malnoy M. 2021.** The
885 *Arabidopsis* pattern recognition receptor EFR enhances fire blight resistance in apple. *Hortic.*
886 *Res.* **8**.
887 **Pixley KV, Falck-Zepeda JB, Paarlberg RL, Phillips PWB, Slamet-Loedin IH, Dhugga KS, Campos H,**
888 **Gutterson N. 2022.** Genome-edited crops for improved food security of smallholder farmers.
889 *Nat. Genet.* **54**(4): 364-367.
890 **Raman V, Rojas CM, Vasudevan B, Dunning K, Kolape J, Oh S, Yun J, Yang L, Li G, Pant BD, et al.**
891 **2022.** *Agrobacterium* expressing a type III secretion system delivers *Pseudomonas* effectors
892 into plant cells to enhance transformation. *Nat. Commun.* **13**(1): 2581.
893 **Ren Q, Sretenovic S, Liu G, Zhong Z, Wang J, Huang L, Tang X, Guo Y, Liu L, Wu Y, et al. 2021.**
894 Improved plant cytosine base editors with high editing activity, purity, and specificity. *Plant*
895 *Biotechnol. J.* **19**(10): 2052-2068.
896 **Roca Paixao JF, Deleris A. 2024.** Epigenetic control of T-DNA during transgenesis and pathogenesis.
897 *Plant Physiol.* **197**(1).
898 **Saur IM, Kadota Y, Sklenar J, Holton NJ, Smakowska E, Belkhadir Y, Zipfel C, Rathjen JP. 2016.**
899 NbCSPR underlies age-dependent immune responses to bacterial cold shock protein in
900 *Nicotiana benthamiana*. *Proc. Natl. Acad. Sci. U. S. A.* **113**(12): 3389-3394.
901 **Schwessinger B, Bahar O, Thomas N, Holton N, Nekrasov V, Ruan D, Canlas PE, Daudi A, Petzold CJ,**
902 **Singan VR, et al. 2015.** Transgenic expression of the dicotyledonous pattern recognition
903 receptor EFR in rice leads to ligand-dependent activation of defense responses. *PLoS Pathog.*
904 **11**(3): e1004809.

905 **Shih PY, Chou SJ, Müller C, Halkier BA, Deeken R, Lai EM. 2018.** Differential roles of glucosinolates
906 and camalexin at different stages of *Agrobacterium*-mediated transformation. *Mol. Plant*
907 *Pathol.* **19**(8): 1956-1970.
908 **Smyth DR, Bowman JL, Meyerowitz EM. 1990.** Early flower development in Arabidopsis. *Plant Cell*
909 **2**(8): 755-767.
910 **Steinert J, Schiml S, Fauser F, Puchta H. 2015.** Highly efficient heritable plant genome engineering
911 using Cas9 orthologues from *Streptococcus thermophilus* and *Staphylococcus aureus*. *Plant J.*
912 **84**(6): 1295-1305.
913 **Suzuki K, Tanaka K, Yamamoto S, Kiyokawa K, Moriguchi K, Yoshida K 2009.** Ti and Ri plasmids. In:
914 Schwartz E ed. *Microbial Megaplasmids*. Berlin, Heidelberg: Springer Berlin Heidelberg, 133-
915 147.
916 **Szarzanowicz MJ, Waldburger LM, Busche M, Geiselman GM, Kirkpatrick LD, Kehl AJ, Tahmin C,**
917 **Kuo RC, McCauley J, Pannu H, et al. 2024.** Binary vector copy number engineering improves
918 *Agrobacterium*-mediated transformation. *Nat. Biotechnol.*
919 **Tiwari M, Mishra AK, Chakrabarty D. 2022.** *Agrobacterium*-mediated gene transfer: recent
920 advancements and layered immunity in plants. *Planta* **256**(2): 37.
921 **van Kregten M, de Pater S, Romeijn R, van Schendel R, Hooykaas PJ, Tijsterman M. 2016.** T-DNA
922 integration in plants results from polymerase-θ-mediated DNA repair. *Nat. Plants* **2**(11):
923 16164.
924 **van Tol N, van Schendel R, Bos A, van Kregten M, de Pater S, Hooykaas PJJ, Tijsterman M. 2022.**
925 Gene targeting in polymerase theta-deficient *Arabidopsis thaliana*. *Plant J.* **109**(1): 112-125.
926 **Wang Y-C, Yu M, Shih P-Y, Wu H-Y, Lai E-M. 2018.** Stable pH suppresses defense signaling and is the
927 key to enhance *Agrobacterium*-mediated transient expression in *Arabidopsis* seedlings. *Sci.*
928 *Rep.* **8**(1): 17071.
929 **Wang Z-P, Xing H-L, Dong L, Zhang H-Y, Han C-Y, Wang X-C, Chen Q-J. 2015.** Egg cell-specific
930 promoter-controlled CRISPR/Cas9 efficiently generates homozygous mutants for multiple
931 target genes in *Arabidopsis* in a single generation. *Genome Biol.* **16**(1): 144.
932 **Weisberg AJ, Wu Y, Chang JH, Lai EM, Kuo CH. 2023.** Virulence and Ecology of Agrobacteria in the
933 Context of Evolutionary Genomics. *Annu. Rev. Phytopathol.* **61**: 1-23.
934 **Wu H-Y, Liu K-H, Wang Y-C, Wu J-F, Chiu W-L, Chen C-Y, Wu S-H, Sheen J, Lai E-M. 2014.** AGROBEST:
935 an efficient *Agrobacterium*-mediated transient expression method for versatile gene
936 function analyses in *Arabidopsis* seedlings. *Plant Methods* **10**(1): 19.
937 **Yang F, Li G, Felix G, Albert M, Guo M. 2023.** Engineered *Agrobacterium* improves transformation by
938 mitigating plant immunity detection. *New Phytol.* **237**(6): 2493-2504.
939 **Ye GN, Stone D, Pang SZ, Creely W, Gonzalez K, Hinchee M. 1999.** *Arabidopsis* ovule is the target for
940 *Agrobacterium* in planta vacuum infiltration transformation. *Plant J.* **19**(3): 249-257.
941 **Yu M, Wang YC, Huang CJ, Ma LS, Lai EM. 2021.** *Agrobacterium tumefaciens* deploys a versatile
942 antibacterial strategy to increase its competitiveness. *J. Bacteriol.* **203**(3): e00490-00420.
943 **Zipfel C, Kunze G, Chinchilla D, Caniard A, Jones JDG, Boller T, Felix G. 2006.** Perception of the
944 bacterial PAMP EF-Tu by the receptor EFR restricts *Agrobacterium*-mediated transformation.
945 *Cell* **125**(4): 749-760.

946

947

948

Figure 1

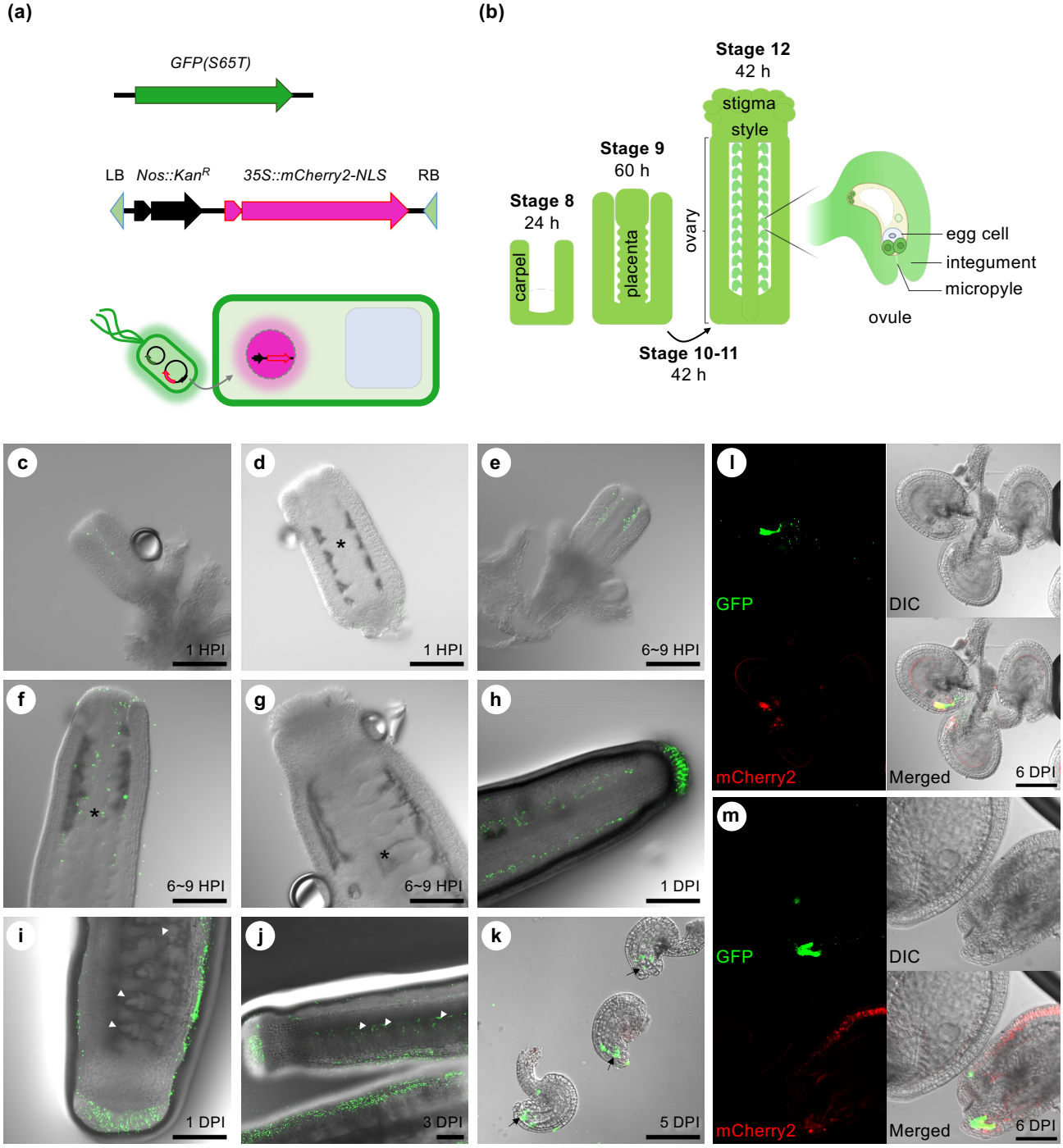

Figure 1. *Agrobacterium* enter open gynoecium within 1 hour but transformation events occur in open flowers after 5 day-post inoculation

(a) *Agrobacterium* GV3101 carrying pRL662-GFP(S65T)/Spe^R and the binary vector 35S::mCherry2-NLS was used for floral inoculation on *Arabidopsis thaliana* Col-0 to visualize *Agrobacterium* localization and transformation events.

(b) Schematic illustration of the structure and development of gynoecium from early to mature stage with stigma, style, ovary containing ovules. The floral stages and their corresponding durations were indicated according to Smyth et al. The diagram was created with BioRender.com.

After one hour-post-inoculation (HPI), *Agrobacterium* cells had already entered the locule of developing gynoecium (c) but were absent in later-stage gynoecia containing developed placenta tissue (d). Between 6-9 HPI, more *Agrobacterium* cells were observed in the locule (e), even at it began to close (f). *Agrobacterium* was not detected in fully closed gynoecia (g).

At one day-post-inoculation (DPI), *Agrobacterium* cells were detected in young closed ovaries (h) but not in older ovaries undergoing ovule development (i). At 3 DPI (j), *Agrobacterium* cells persisted in ovaries at late developmental stages. By 5 DPI, *Agrobacterium* cells were enriched around the micropyle (arrow) (k), though no mCherry2 signal was detected. At floral open stage after 6 DPI, *Agrobacterium* accumulated around the micropyle, and mCherry2 signal became visible (l and m).

Asterisks (*) indicate placenta tissue; arrowheads denote developing ovule; arrows indicate *Agrobacterium* located around micropyle. Panels (a to k) were merged channel images; panels (l and m) show GFP, mCherry2, DIC and merged views. Scale bar= 100 µm.

Figure 2

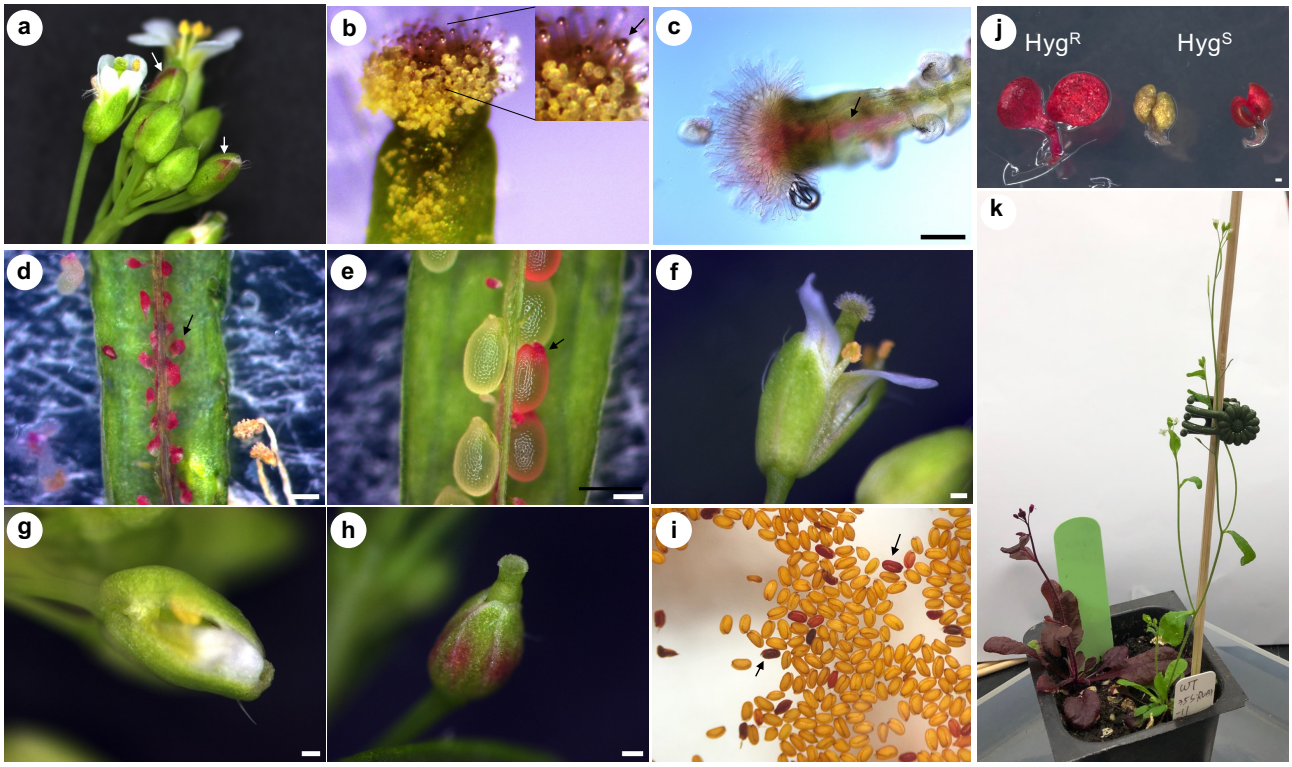

Figure 2. RUBY marker revealed transformation events in floral organs and female tissues
RUBY signals were observed in flowers (a), specifically on the stigma but not on pollen grains (b), and in the transmitting tissue (c). In siliques, RUBY expression was detected in both abortive (d) and developing ovules (e).

Flower morphology after AMT-FI ranged from normal open flowers (f) to partially open flowers (g), and flowers with only gynoecia emerging from sepals (h).

RUBY signal intensity varied among seeds (i) and plants (j, k). (j) At the seedling stage, hygromycin-resistant (Hyg^R) and RUBY-positive seedling (left), non-transgenic seedling (middle), and RUBY-positive but hygromycin-sensitive (Hyg^S) seedling (right) were observed. (k) Transgenic T1 plants with variable RUBY expression patterns from strong whole-plant expression to undetectable signal. Scale bar = 200 μm.

Figure 3

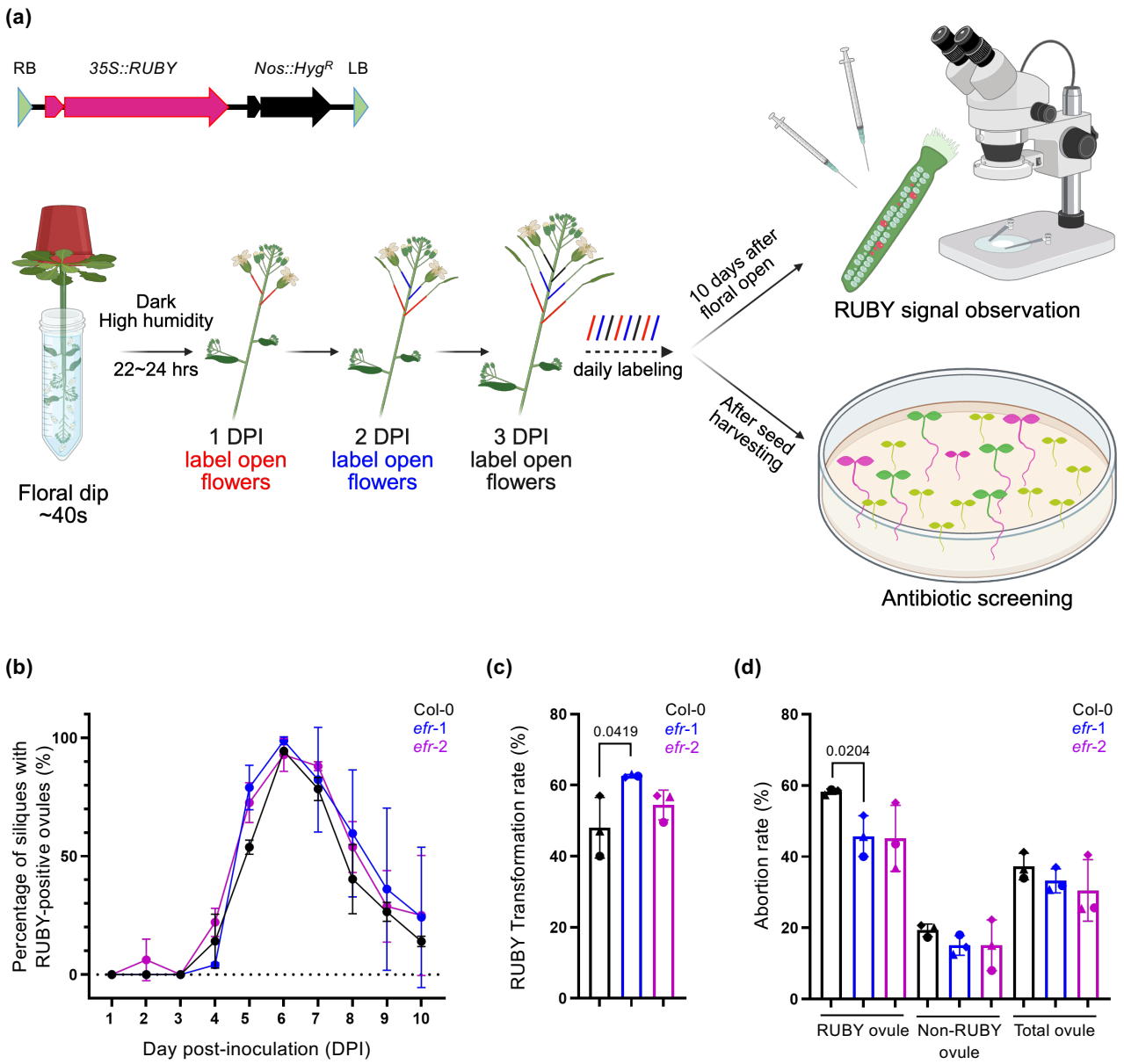

Figure 3. *Agrobacterium* infection and EFR-mediated immunity exert negative impacts on ovule development
(a) Experimental design: a schematic diagram illustrates the 35S::RUBY construct and experimental workflow. Transformation efficiency was evaluated based on the presence of RUBY-positive ovules and hygromycin-resistant seedlings. The diagram was created with BioRender.com.

(b) Percentage of siliques with RUBY-positive ovules recorded daily for Col-0 WT, *efr*-1, and *efr*-2 from flowers that opened at 1-10 DPI. Data are mean ± SD of three biological replicates from two independent experiments.

(c) RUBY-based transformation. Percentage of RUBY-positive ovules (include both developed and abortive ovules) per silique collected from flowers of Col-0 WT, *efr*-1 and *efr*-2 opened at 5-9 DPI was calculated (all data points shown in Fig. S3a). Data are mean ± SD of average percentage of RUBY-positive ovules from three independent experiments (circle, triangle and rhombus symbols). Statistically significant differences ($p < 0.05$) between Col-0 WT and efr mutants are indicated.

(d) Ovule abortion rate. The abortion rate of RUBY-positive, non-RUBY, and total ovules per silique collected from flowers of Col-0 WT, *efr*-1 and *efr*-2 opened at 5-9 DPI was calculated (all data points shown in Fig. S3c). Data are mean ± SD of average abortion rate from three independent experiments (circle, triangle and rhombus symbols). Statistically significant differences ($p < 0.05$) between Col-0 WT and efr mutants are indicated.

Figure 4

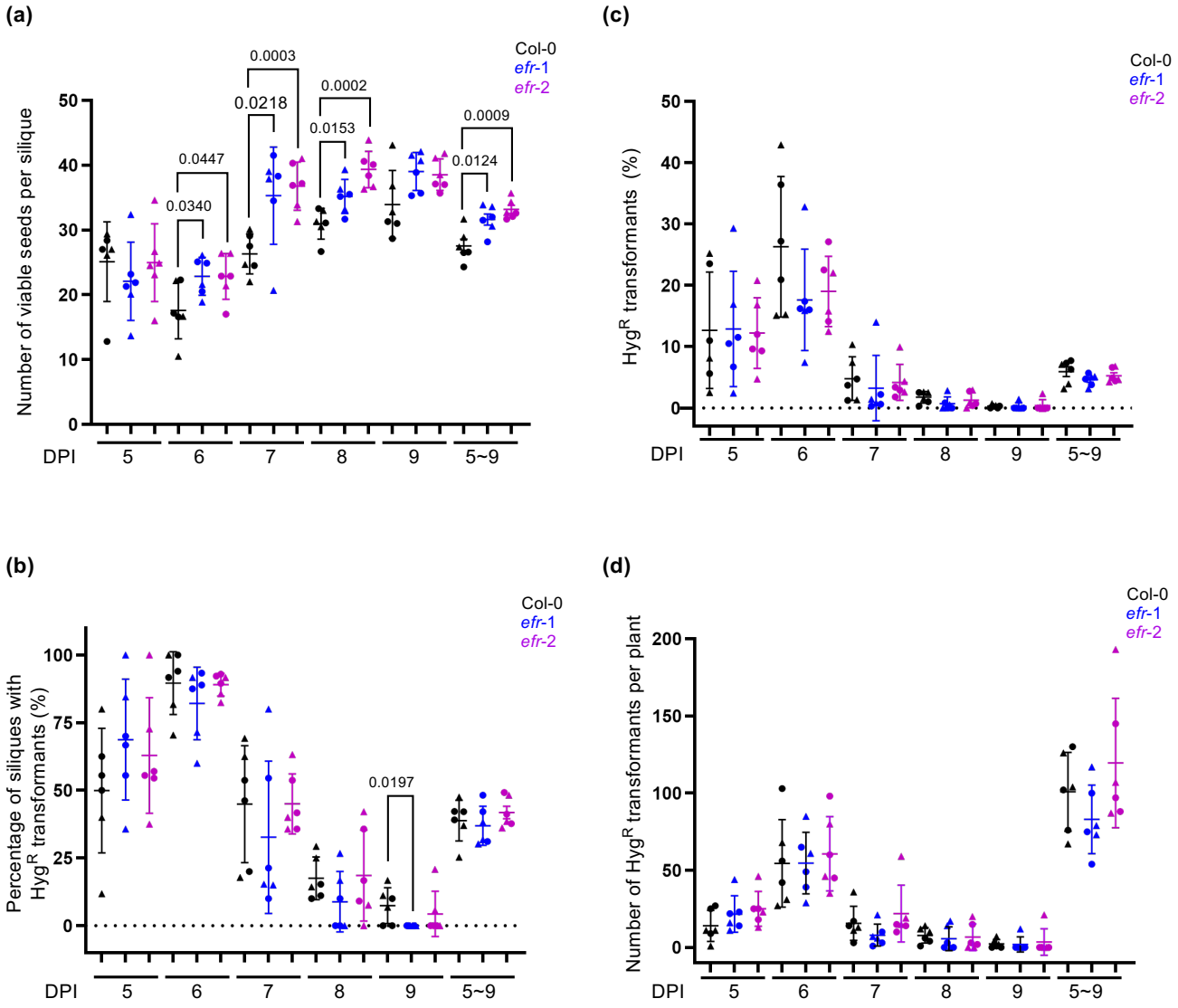

Figure 4. AMT events occur mainly in flowers opened at 5-9 DPI, peaking at 6 DPI
Siliques and seeds developed from flowers that opened at 5-9 DPI in Col-0 WT, *efr*-1 and *efr*-2 mutants were analyzed through viability (a) and hygromycin resistance (Hyg^R) screening (b, c, d) and viability (d). Data are (a) average number of viable seeds per silique, (b) percentage of siliques containing Hyg^R transformants, (c) percentage of Hyg^R transformants and (d) number of Hyg^R transformants per plant. Data are mean ± SD of six biological replicates from two independent experiments (circle and triangle symbols). Statistically significant differences ($p < 0.05$) between Col-0 WT and *efr* mutants are indicated.

Figure 5

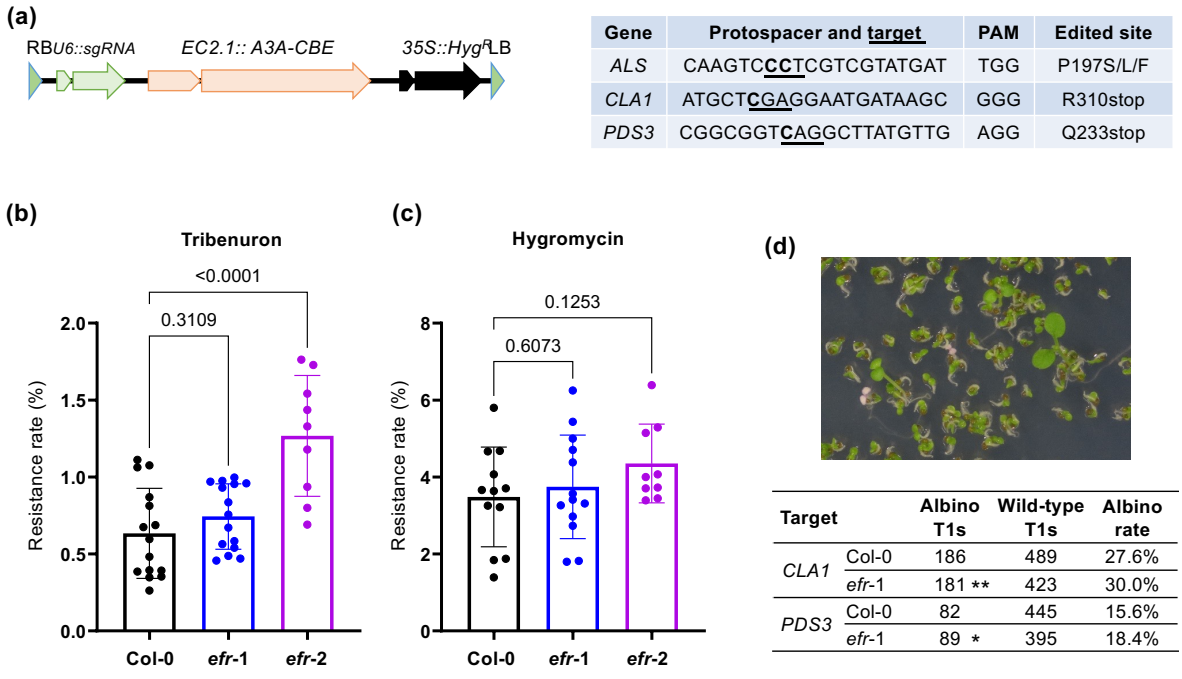

Gene	Protospacer and target	PAM	Edited site
ALS	CAAGTC**CC**TCGTCGTATGAT	TGG	P197S/L/F
CLA1	ATGCT**C**GAGGAATGATAAGC	GGG	R310stop
PDS3	CGGCGGT**C**AGGCTTATGTTG	AGG	Q233stop

Target		Albino T1s	Wild-type T1s	Albino rate
CLA1	Col-0	186	489	27.6%
	efr-1	181 **	423	30.0%
PDS3	Col-0	82	445	15.6%
	efr-1	89 *	395	18.4%

Figure 5. EFR suppresses genome editing efficiency
Agrobacterium GV3101 carrying a binary vector encoding a base editor and a sgRNA was used for floral inoculation in Col-0 WT and *efr* mutants to assess genome editing and stable transformation efficiencies.

(a) A schematic diagram of the binary vector structure for base editing and target gene information.

(b) Genome editing efficiency assessed by tribenuron-resistant T1 plants with targeting the *ALS* Pro197 locus.

(c) Stable transformation efficiency evaluated by hygromycin resistance.

(b) and (c): Seeds are collected from flowers that opened at 5-9 DPI. Each data point represents biological replicates from six independent experiments. Data are mean ± SD, with *p*-values calculated by Student's t-test between Col-0 WT and *efr* mutants.

(d) Genome editing efficiency assessed based on albino phenotype in T1 plants, resulting from by loss-of-function mutations at locus *CLA1 and PDS3.* Statistically significant differences between Col-0 WT and *efr* are indicated (*$p < 0.05$, **$p < 0.01$, chi-square analysis).

Figure 6

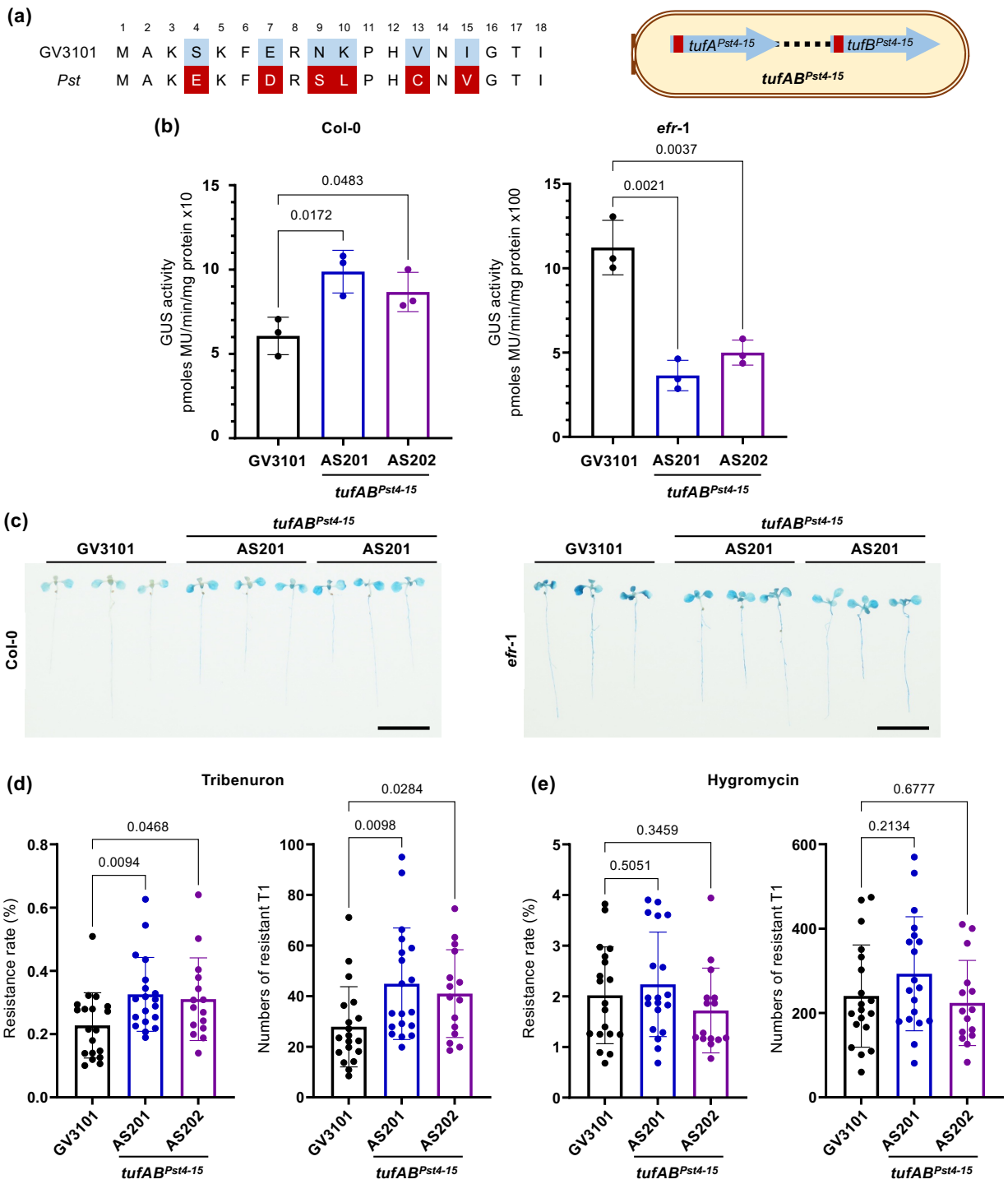

Figure 6. Modification of *Agrobacterium* EF-Tu enhances transient gene expression and genome editing efficiency but not stable T-DNA integration efficiency

The two engineered *Agrobacterium tufAB*$^{Pst4-15}$ strains, AS201 and AS202, were assessed for its efficiency in transient expression, genome editing, and stable transformation in comparison to the parental *Agrobacterium* GV3101.

(a) A schematic diagram illustrating the difference of *tufAB* sequences at amino acids 4th to 15th between *Agrobacterium* GV3101 and *Pseudomonas syringae* (*Pst*).

(b, c) Comparison of transient transformation efficiencies between the GV3101 WT and two *tufAB*$^{Pst4-15}$ strains (AS201 and AS202) in *A. thaliana* seedlings by quantitative GUS activity (b) GUS staining (c, scale bar =1 cm). Results are representative of three independent experiments.

(d) Comparison of genome editing efficiency between the GV3101 WT and two *tufAB*$^{Pst4-15}$ strains (AS201 and AS202) measured by the percentage of tribenuron-resistant T1 plants (left) and number of edited T1 plants per three T0 plants (right).

(e) Comparison of stable transformation efficiency by the number of hygromycin-resistant T1 plants per three T0 plants, with no significant differences between WT GV3101 and the two *tufAB*$^{Pst4-15}$ strains (AS201 and AS202).

Seeds were collected from all flowers. Each data point represents biological replicates from three independent experiments. All values are shown as mean ± SD, with *p*-values calculated by Student's t-test.

Figure 7

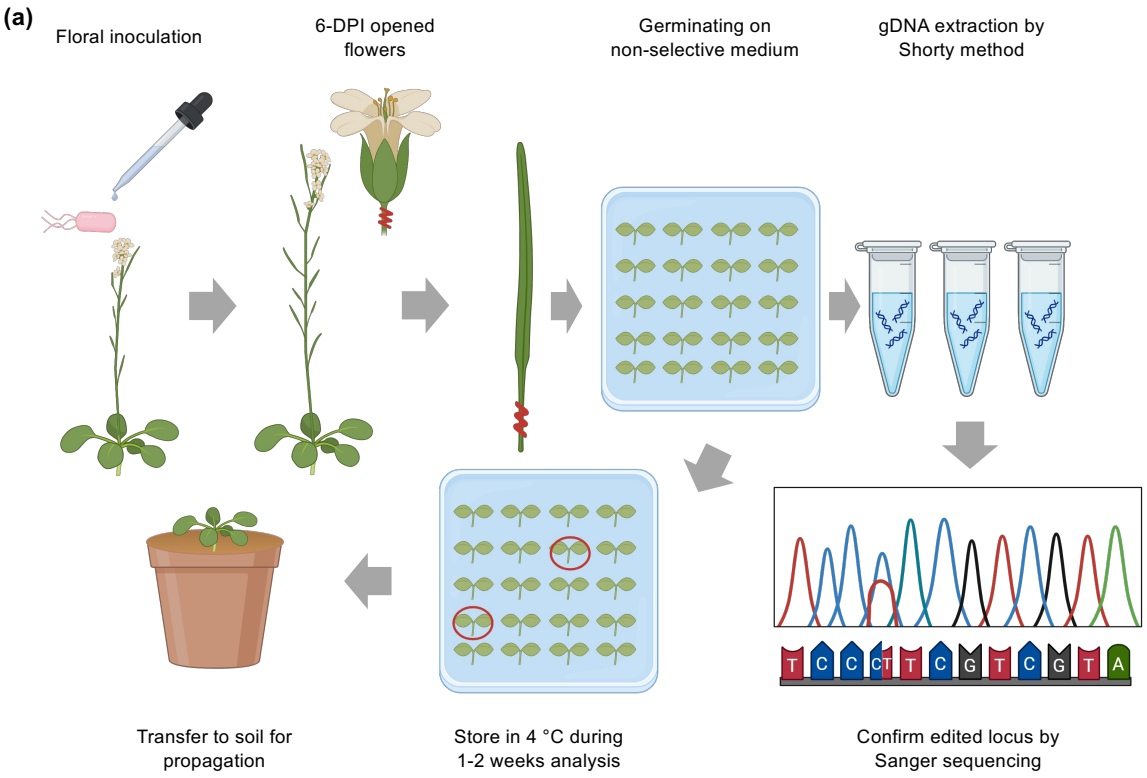

(b)

Plants	Col-0	*efr*-1	*efr*-2	Col-0	*efr*-1	*efr*-2	Col-0	Col-0
AMT-FI strain	GV3101	GV3101	GV3101	GV3101	GV3101	GV3101	GV3101	AS201
Target	*CLA1*	*CLA1*	*CLA1*	*CLA1*	*CLA1*	*CLA1*	*ALS*	*ALS*
Numbers of analyzed progenies of T0	212	188	236	64	63	64	94	93
GE confirmation	Albino seedling			Sanger sequencing			Sanger sequencing†	
Numbers of edited T1	7	7	10	1	10*	3	1	2
GE rate	3.30%	3.72%	4.24%	1.56%	15.87%	4.69%	1.06%	2.15%

Figure 7. Sequencing-based screening of genome-edited plants
(a) Workflow for screening genome-edited T1 plants from flowers that opened at 6 DPI. Seeds were germinated in 1/2 MS medium with only supplemented with timentin to suppress *Agrobacterium* growth without hygromycin selection. 10-day-old T1 plants were analyzed by Sanger sequencing at the *ALS* or *CLA1* loci. The diagram was created with BioRender.com.

(b) The number of sequenced T1 plants and editing rates. †indicates the C to T editing at Pro197 locus conferring tribenuron resistance. Statistically significant differences in genome editing (GE) rates between *efr*-1 and WT Col-0 are indicated (*$p < 0.001$, chi-square analysis).

Supplemental figure 1

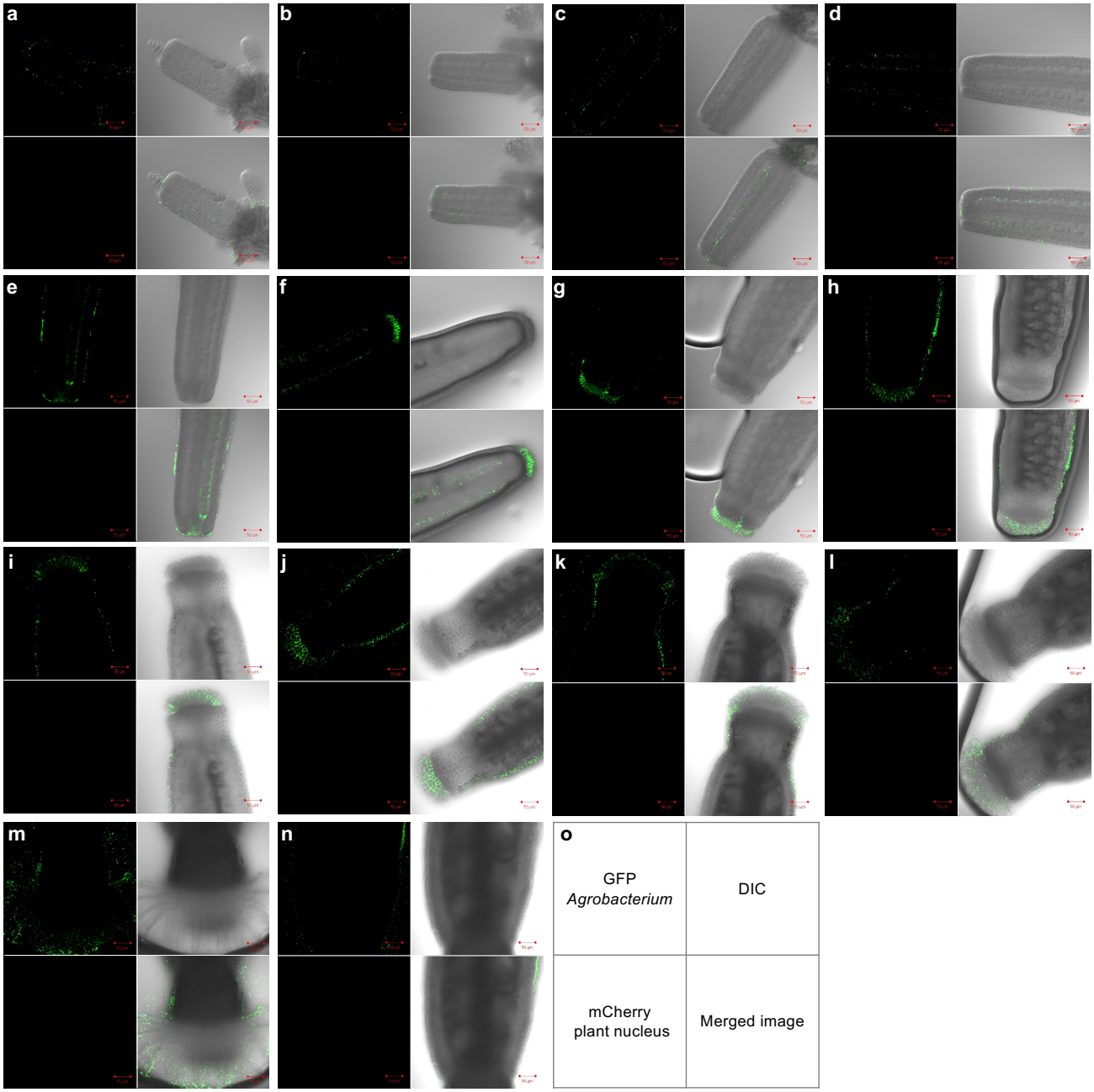

Figure S1. Basipetal analysis of *Agrobacterium* distribution along *Arabidopsis* inflorescence at 1 DPI.
A basipetal series of flowers from the inflorescence tip (a) to the first open flower at the base (m and n) were dissected to visualize distribution of *Agrobacterium* expressing GFP reporter at 1 DPI. The order was determined in considering the position and developmental stage of flowers. Each figure consists of four imaging channels (o). Scale bars indicated 50 µm. Panels a-e show open gynoecia, f-n are closed gynoecia, m and n are from different regions of the same flower.

Supplemental figure 2

(a)

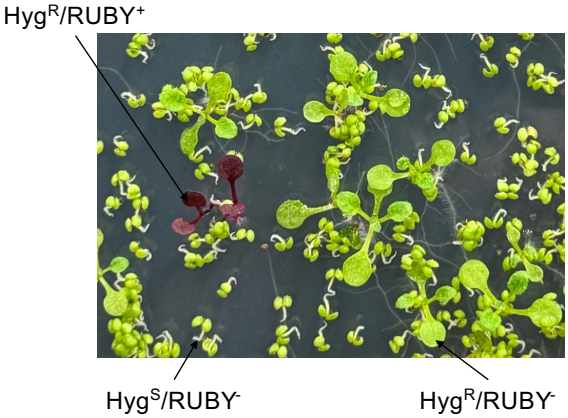

(b)

Genotype	Number of Hyg^{R} T1		
	Total	RUBY^{+}	Percentage of RUBY^{+}
Col-0 WT #1	67	4	6.0%
Col-0 WT #2	89	6	6.7%
Col-0 WT #3	48	3	6.3%
efr-1 *#1*	124	11	8.9%
efr-1 *#2*	129	15	11.6%
efr-2 *#1*	107	7	6.5%
efr-2 *#2*	117	11	9.4%

Figure S2. Number and percentage of Hyg^{R}/RUBY^{+} T1 seedlings
(a) Representative photo of T1 seedlings screening on hygromycin containing 1/2 MS plate. The hygromycin-resistant T1 exhibiting RUBY signals of whole seedling (Hyg^{R}/RUBY^{+}) was indicated, among the hygromycin-resistant green and larger T1 seedling (Hyg^{R}/RUBY^{-}), and hygromycin-sensitive green but small seedlings (Hyg^{s}/RUBY^{-}). The hygromycin-sensitive T1 seedlings with RUBY signals (Hyg^{s}/RUBY^{+}) shown in Fig. 2j are rarely occurred and not present in this photo.

(b) Number and percentage of Hyg^{R}/RUBY^{+} T1 seedlings in Col-0 WT and *efr* mutants. Total number of Hyg^{R} T1 seedlings (Total) and those exhibiting RUBY signals of whole seedling (RUBY^{+}) was indicated and the percentage of Hyg^{R}/RUBY^{+} T1s among total Hyg^{R} T1s.

Supplemental figure 3

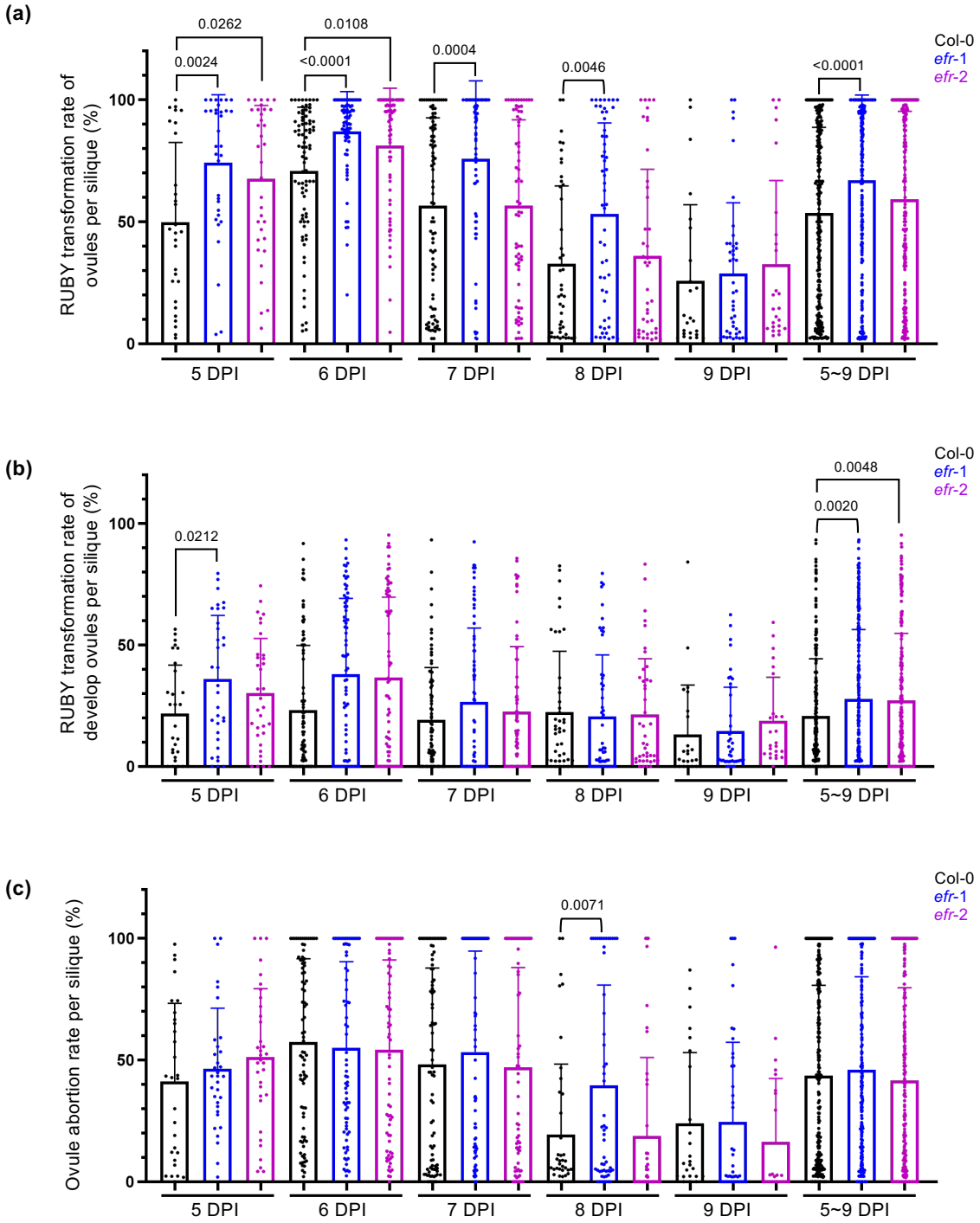

Figure S3. EFR-mediated immunity exerts negative impacts on ovule development and RUBY-based transformation rate

GV3101 carrying the 35S::RUBY construct was used for AMT-FI to assess RUBY-based transformation efficiency and ovule abortion rate in Col-0 WT and *efr* mutants. Siliques from flowers that opened at 5-9 DPI were analyzed to count the total number of ovules, the number of developed ovules with or without RUBY signals, and the number of abortive ovules with or without RUBY signals per silique. Related to Figure 3.

(a) Daily RUBY-based transformation rate per silique. The percentage of RUBY-positive ovules (including both developed and abortive ovules) per silique was calculate at each DPI, as well as cumulatively across 5-9 DPI. Each data point represents the percentage of RUBY-positive ovules per silique.

(b) Daily RUBY-based transformation rate of developed ovules per silique. The percentage of RUBY-positive developed (non-abortive) ovules per silique was measured at each DPI, as well as cumulatively across 5-9 DPIs. Each data point represents the percentage of RUBY-positive developed ovules per silique.

(c) Daily ovule abortion rate per silique. The percentage of abortive ovules (including both RUBY-positive and RUBY-negative) per silique was recorded at each DPI and cumulatively across 5-9 DPI. Each data point represents the percentage of abortive ovules per silique.

Data are shown in mean ± SD from three independent experiments, with p values calculated by Student's t-test between Col-0 WT and *efr* mutants.

Supplemental figure 4

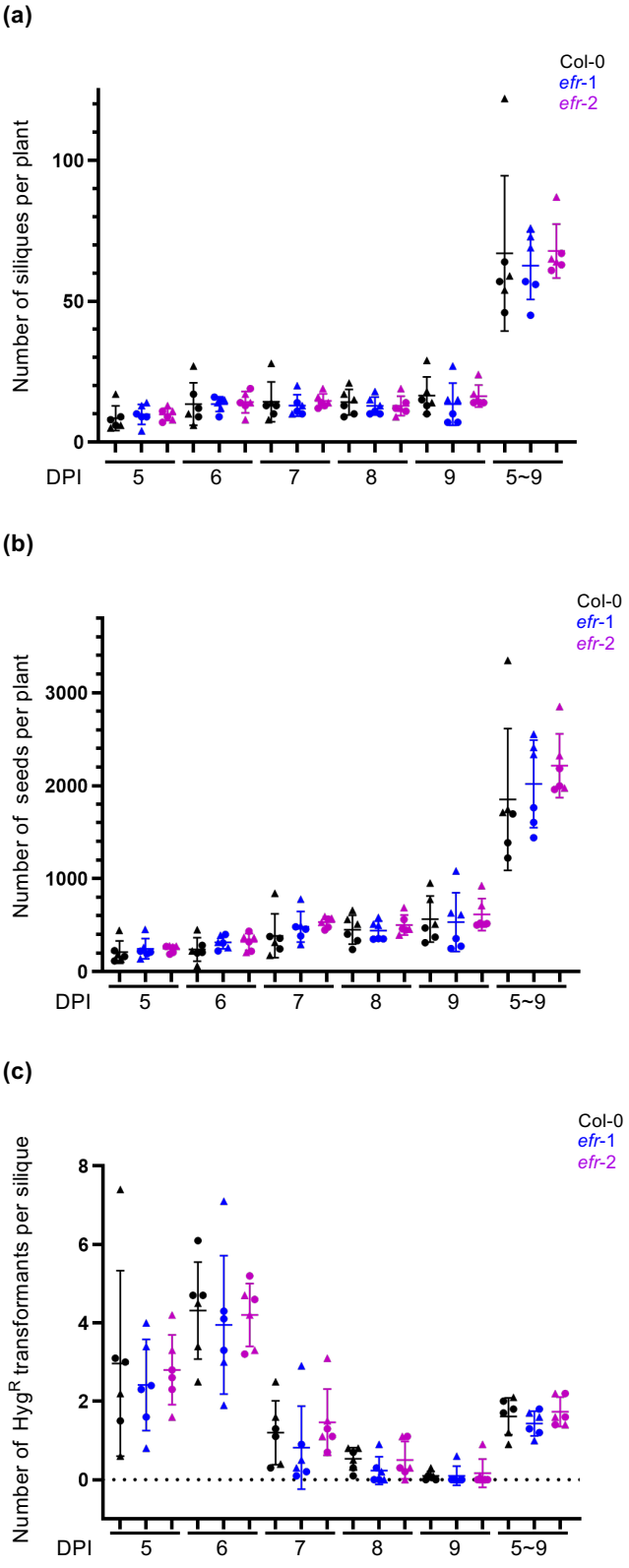

Figure S4. Number of siliques, seeds, and hygromycin-resistant seedlings in Col-0 WT, *efr*-1 and *efr*-2 mutants after AMT-FI
Siliques and seeds developed from flowers that opened at 5-9 DPI in Col-0 WT, *efr*-1 and *efr*-2 mutants were analyzed through number of siliques (a) and seeds (b) per plant, and averaged number of hygromycin-resistant (Hyg^R) seedlings per silique (c). Data are mean ± SD of six biological replicates from two independent experiments (circle and triangle symbols).

Supplemental figure 5

(a)

Number of Developed Seeds							Percentage of Developed Seeds after infection		
Treatment	Infiltration Medium (IM)			IM+GV3101					
Genotype	Col-0	*efr*-1	*efr*-2	Col-0	*efr*-1	*efr*-2	Col-0	*efr*-1	*efr*-2
Mean	35.6	42.7	44.5	29.4	37.4	40.6	82.6%	87.6%	91.2%
SD	13.1	9.2	11.0	16.3	14.0	12.8			
Number of Germinated Seeds (Germination Rate)							**Percentage of Germinated seeds after infection**		
Treatment	Infiltration Medium (IM)			IM+GV3101					
Genotype	Col-0	*efr*-1	*efr*-2	Col-0	*efr*-1	*efr*-2	Col-0	*efr*-1	*efr*-2
Mean	35.5 (99.7%)	42.5 (99.5%)	44.3 (99.6%)	26.4 (89.8%)	34.4 (92.0%)	36.7 (90.4%)	74.4%	80.9%	82.8%
SD	13.2	9.2	11.1	17.9	15.5	14.4			

(b)

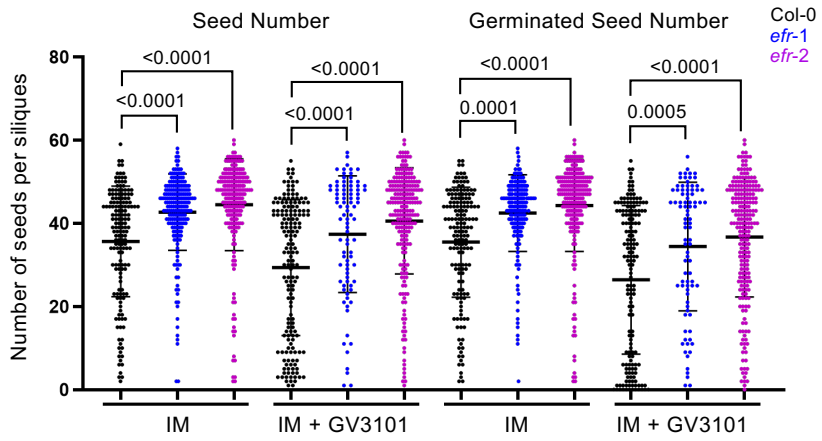

Figure S5. *Agrobacterium* infection and EFR-mediated immunity affect seed outputs.
(a) Table showing seed number per silique from plants treated with infiltration medium alone or with *Agrobacterium.* Percentage of developed/germinated seeds after infection was normalized to those from infiltration medium (IM) treatment. The resulting percentage of developed and germinated seeds indicated the impact on seed viability.

(b) Seed counts and germination rates following IM alone or with *Agrobacterium* IM (IM + GV3101) treatments. Siliques were collected from flowers that opened at 5–9 DPI. The total number of seeds and the number of germinated seeds were compared between treatments.

Data were collected from two plants per genotype, except for *efr-1* infected with GV3101, where data were obtained from one plant. Data are shown as mean ± SD, with *p*-values calculated using Student's *t*-test to compare *Col-0* WT and *efr* mutants.

Supplemental figure 6

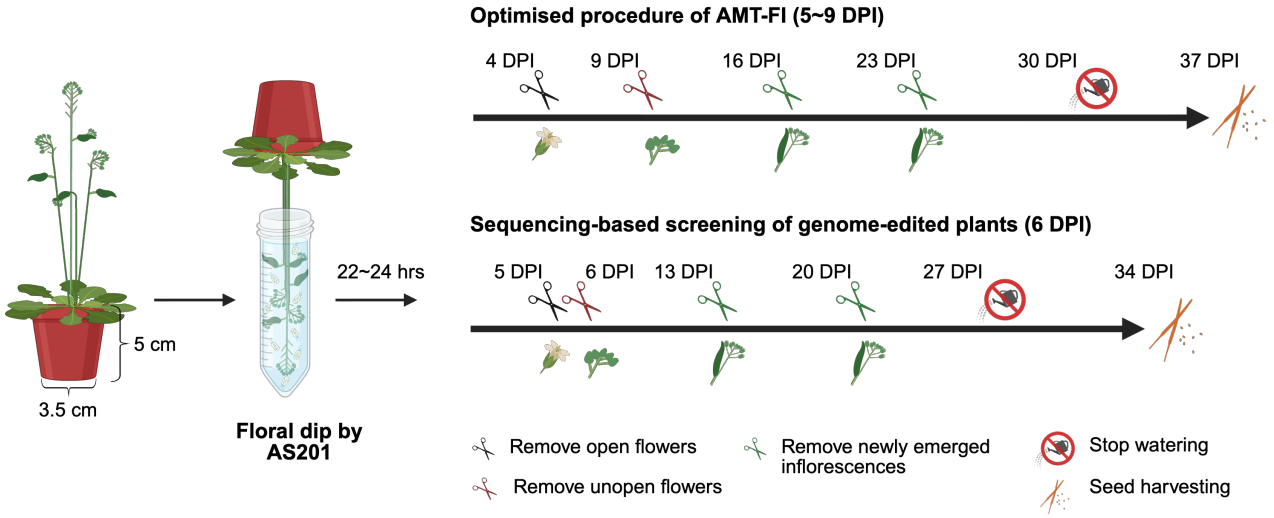

Figure S6. The recommended AMT-FI procedure.
The experimental procedures for achieving higher AMT-FI efficiency and for screening genome-edited T1 plants without prior selection for T-DNA integration are illustrated. The engineered *tufAB*-modified strain AS201 is recommended for plant transformation in *A. thaliana or other plant species possessing EFR. The optimized transformation window was determined under the growth conditions of A. thaliana, with each plant cultivated in a small pot (5 cm upper diameter × 5 cm height × 3.5 cm bottom diameter). The diagram was created with BioRender.com.*

Supplemental Table 1. Strain and Plasmid information

Lab collection #	***Agrobacterium* strain**/ Plasmid/ Antibiotics resistance	Characteristics	Source
EML485	**GV3101**/Rif^{R}Gen^R	GV3101 containing pMP90, which is pTiC58 derivative with T-DNA deletion and gentamicin resistance gene	Koncz and Schell, 1986
EML8561	**AS201**/ Rif^{R}Gen^R	GV3101::*tufAB*$^{Pst4-15}$ mutant by modifying *tufB* followed by *tufA*, with both genes encoding a chimeric EF-Tu with amino acids 4-15 from corresponding *Pst* EF-Tu	This study
EML8559	**AS202**/ Rif^{R}Gen^R	GV3101::*tufAB*$^{Pst4-15}$ mutant by modifying *tufA* followed by *tufB*, with both genes encoding a chimeric EF-Tu with amino acids 4-15 from corresponding *Pst* EF-Tu	This study
EML3375	pRL662-GFP(S65T)/ Gen^R	Broad host range plasmid confers gentamycin resistance and expression of GFP(S65T)	Yu et al., 2021
EML6428	pRL662-GFP(S65T)/Spe^R	Broad host range plasmid confers spectinomycin resistance and expression of GFP(S65T)	This study, Addgene#234350
EML6409	35S::RUBY/Spe^R	Binary vector carrying T-DNA expressing RUBY reporter and hygromycin resistance	Addgene#160908
EML6442	35S:mCherry2-NLS/Kan^R	Binary vector carrying T-DNA expressing mCherry2 florescent proteins	This study, Addgene#234351
EML8357	pA3A-CBECas9/Kan^R	Binary vector carrying T-DNA expressing base editor driven by egg-cell specific promoter	This study, Addgene#234352
EML8359	pA3A-CBECas9-Pro197/Kan^R	Binary vector carrying T-DNA expressing base editor targeting *ALS Pro197* locus	This study, Addgene#234353
EML8532	pA3A-CBECas9-CLA1/Kan^R	Binary vector carrying T-DNA expressing base editor targeting *CLA1*, generating early stop codon	This study
EML8533	pA3A-CBECas9-PDS3/Kan^R	Binary vector carrying T-DNA expressing base editor targeting *PDS3*, generating early stop codon	This study
EML121	pJQ200KS/Gen^R	Suicide plasmid contains *sacB* and Gm^R *traJ oriT* for the selection of double crossover events	Quandt and Hynes, 1993
EML8543	pEML041003/Kan^R	pJQ200KS derived suicide vector for gene replacement in *Agrobacterium*	This study, Addgene#237864
EML8552	pEML041003-tufAPst4-15/ Kan^R	Suicide vector for replacing 4th to 15th amino acids of *tufA*	This study, Addgene#237865
EML8553	pEML041003-tufBPst4-15/ Kan^R	Suicide vector for replacing 4th to 15th amino acids of *tufB*	This study, Addgene#237866

Gen^R, gentamycin resistance; Kan^R, kanamycin resistance; Rif^R, rifampicin resistance; Spe^R, spectinomycin resistance

Supplemental Table 2. Primer information

Primers	5' to 3' sequence	R.E. site	Source
Cloning of pRL662-GFP(S65T) with spectinomycin resistance			
Spe_F	GTCGATGTTTGATGTTATGGAGCAGCAACGATGGGGGAAGCGGTGATCGCCGAAGTATCG		This study
Spe_R	CGGGAAGCCGATCTCGGCTTGAACGAATTGTTATTTGCCGACTACCTTGGTGATCTCGCC		
662_F	CGATACTTCGGCGATCACCGCTTCCCCCATCGTTGCTGCTCCATAACATCAAACATCGAC		This study
662_R	GGCGAGATCACCAAGGTAGTCGGCAAATAACAATTCGTTCAAGCCGAGATCGGCTTCCCG		
Cloning of binary vector with 35S:mCherry2-NLS			
MC2-F	AAGGTCTCAAATGGTGAGTAAAGGAGAAGA	BsaI	This study
MC2-R	AAGGTCTCAAAGCTTAGGCGCCTACCTTTCTCTTCTTTTTTGGGCCTTTGTATAGTTCATCCATGCCACC	BsaI	
Cloning of protospacer			
Pro197-fw	ATTG CAAGTCCCTCGTCGTATGAT		Chen et al., 2017
Pro197-rv	AAAC ATCATACGACGAGGGACTTG		
CLA1-fw	ATTG ATGCTCGAGGAATGATAAGC		Liu et al., 2022
CLA1-rv	AAAC GCTTATCATTCCTCGAGCAT		
PDS3-fw	ATTG CGGCGGTCAGGCTTATGTTG		Liu et al., 2022
PDS3-rv	AAAC CAACATAAGCCTGACCGCCG		
Double crossover vector for cloning *tufA*$^{Pst4\text{-}15}$ and *tufB*$^{Pst4\text{-}15}$			
tufA-1f	TTGGTCTCAGGAGCACGATCTTGCGGATGC	BsaI	This study
tufA-1r	AGGTCTCGCCCTCCCGCATTGCAACGTCGGCACGATCGGTCACGTCG	BsaI	
tufA-2f	AGGTCTCGAGGGAACGATCAAATTTTTCCTTTGCCATGTGAATTGCTTCC	BsaI	
tufA-2r	AAGGTCTCGAGCGCAGTTCCGTCCACATCTTC	BsaI	
tufB-1f	TTGGTCTCAGGAGTTAGAGCTTGATTTCCACGTCAA	BsaI	
tufB-1r	AGGTCTCGCCCTCCCGCATTGCAACGTCGGCACGATCGGTCACGTCG	BsaI	
tufB-2f	AGGTCTCGAGGGAACGATCAAATTTTTCCTTTGCCATTAGTGGCTCTCC	BsaI	
tufB-2r	AAGGTCTCGAGCGTTCGAACCGAACCCTGA	BsaI	

References

Chen, Y., Wang, Z., Ni, H., Xu, Y., Chen, Q. and Jiang, L. (2017) CRISPR/Cas9-mediated base-editing system efficiently generates gain-of-function mutations in *Arabidopsis*. *Sci. China Life Sci.* **60**, 520-523.

Koncz, C. and Schell, J. (1986) The promoter of TL-DNA gene 5 controls the tissue-specific expression of chimaeric genes carried by a novel type of *Agrobacterium* binary vector. *Molec. Gen. Genet.* **204**, 383-396.

Liu, D., Xuan, S., Prichard, L.E., Donahue, L.I., Pan, C., Nagalakshmi, U., Ellison, E.E., Starker, C.G., Dinesh-Kumar, S.P., Qi, Y. and Voytas, D.F. (2022) Heritable base-editing in *Arabidopsis* using RNA viral vectors. *Plant Physiol.* **189**, 1920-1924.

Quandt, J. and Hynes, M.F. (1993) Versatile suicide vectors which allow direct selection for gene replacement in Gram-negative bacteria. *Gene* **127**, 15-21.

Yu M, Wang YC, Huang CJ, Ma LS, Lai EM. 2021. *Agrobacterium tumefaciens* deploys a versatile antibacterial strategy to increase its competitiveness. J Bacteriol 203:10.1128/jb. 00490-20.